NAVAL POSTGRADUATE SCHOOL
MONTEREY, CALIFORNIA

THESIS

SMALL-SCALE MORPHOLOGY RELATED TO WAVE AND CURRENT PARAMETERS ACROSS THE SURF ZONE

by

Jeffrey Lynn Swayne

December, 1995

Thesis Advisor: E.B. Thornton

Approved for public release; distribution is unlimited.

DISCLAIMER NOTICE

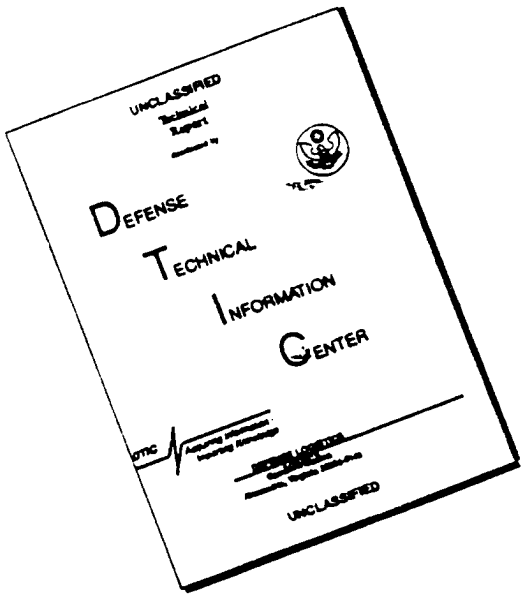

THIS DOCUMENT IS BEST QUALITY AVAILABLE. THE COPY FURNISHED TO DTIC CONTAINED A SIGNIFICANT NUMBER OF PAGES WHICH DO NOT REPRODUCE LEGIBLY.

REPORT DOCUMENTATION PAGE

Form Approved OMB No. 0704-0188

1. AGENCY USE ONLY *(Leave blank)*	2. REPORT DATE December 1995	3. REPORT TYPE AND DATES COVERED Master's Thesis

4. TITLE AND SUBTITLE SMALL-SCALE MORPHOLOGY RELATED TO WAVE AND CURRENT PARAMETERS ACROSS THE SURF ZONE

5. FUNDING NUMBERS

6. AUTHOR(S) Swayne, Jeffrey Lynn

7. PERFORMING ORGANIZATION NAME(S) AND ADDRESS(ES)
Naval Postgraduate School
Monterey CA 93943-5000

8. PERFORMING ORGANIZATION REPORT NUMBER

9. SPONSORING/MONITORING AGENCY NAME(S) AND ADDRESS(ES)
Office of Naval Research
Coastal Sciences

10. SPONSORING/MONITORING AGENCY REPORT NUMBER

11. SUPPLEMENTARY NOTES The views expressed in this thesis are those of the author and do not reflect the official policy or position of the Department of Defense or the U.S. Government.

12a. DISTRIBUTION/AVAILABILITY STATEMENT
Approved for public release; distribution is unlimited.

12b. DISTRIBUTION CODE

13. ABSTRACT *(maximum 200 words)*

Small-scale beach morphology (scales < 5 m) height variations were measured by combining the CRAB survey with bed elevation acquired from a 1 MHZ sonic altimeter mounted on the CRAB during the October phase of the DUCK94 experiment. Bedform types were observed using a 500 kHZ side-scan sonar also mounted on the CRAB. Corollary waves and currents were measured. Three cases were examined in detail: mild waves and weak longshore currents resulting in wave ripples everywhere; storm waves with strong longshore currents resulting in lunate and straight crested megaripples in the trough of the barred beach; and narrow banded, normally incident waves with a strong rip current resulting in a relatively planar bed everywhere except in the throat of the rip where magaripples were measured. The predictive wave ripple height and length equations of Nielsen (1981) worked reasonably well for mild wave conditions, but did not predict ripples during moderate wave conditions. The wavenumber spectra were generally broad, indicating that newly formed ripples coexisted with residual ripples from the past to form complex, multi-scaled ripple patterns.

14. SUBJECT TERMS nearshore, small-scale morphology, bathymetry, megaripples			15. NUMBER OF PAGES 74
			16. PRICE CODE
17. SECURITY CLASSIFICATION OF REPORT Unclassified	18. SECURITY CLASSIFICATION OF THIS PAGE Unclassified	19. SECURITY CLASSIFICATION OF ABSTRACT Unclassified	20. LIMITATION OF ABSTRACT UL

NSN 7540-01-280-5500

Standard Form 298 (Rev. 2-89)
Prescribed by ANSI Std. 239-18 298-102

Approved for public release; distribution is unlimited.

SMALL-SCALE MORPHOLOGY RELATED TO WAVE AND CURRENT PARAMETERS ACROSS THE SURF ZONE

Jeffrey Lynn Swayne
Lieutenant, United States Navy
B.S., Pennsylvania State University, 1983

Submitted in partial fulfillment
of the requirements for the degree of

MASTER OF SCIENCE IN METEOROLOGY AND PHYSICAL OCEANOGRAPHY

from the

NAVAL POSTGRADUATE SCHOOL
December 1995

Author: Jeffrey Lynn Swayne
Jeffrey Lynn Swayne

Approved by: Edward B. Thornton
Edward B. Thornton, Thesis Advisor

Thomas H. C. Herbers, Second Reader

Robert H. Bourke, Chairman
Department of Oceanography

ABSTRACT

Small-scale beach morphology (scales < 5 m) height variations were measured by combining the CRAB survey with bed elevation acquired from a 1 MHZ sonic altimeter mounted on the CRAB during the October Phase of the DUCK94 experiment. Bedform types were observed using a 500 kHz side-scan sonar also mounted on the CRAB. Corollary waves and currents were measured. Three cases were examined in detail: mild waves and weak longshore currents resulting in wave ripples everywhere; storm waves with strong longshore currents resulting in lunate and straight crested megaripples in the trough of the barred beach; and narrow banded, normally incident waves with a strong rip current resulting in a relatively planar bed everywhere except in the throat of the rip where megaripples were measured. The predictive wave ripple height and length equations of Nielsen (1981) worked reasonably well for mild wave conditions, but did not predict ripples during moderate wave conditions. The wavenumber spectra were generally broad, indicating that newly formed ripples coexisted with residual ripples from the past to form complex, multi-scaled ripple patterns.

TABLE OF CONTENTS

LIST OF FIGURES

ACKNOWLEDGMENTS

This research was funded by the Office of Naval Research, Coastal Sciences Program, under contract N00114-95-AF-0002. The author wishes to express his sincere appreciation to Prof. Edward B. Thornton for his support and guidance throughout the thesis process. I would also like to thank all those who participated in DUCK94 experiment, namely the staff of the U.S. Army Field Research Facility under the direction of B. Birkemeier. The loan of the sonic altimeter by S. Elgar, Washington State University, is greatly appreciated. In addition, special appreciation is expressed to R. Wyland, Naval Postgraduate School, for his role in the acquisition of wave and current data, and to Mary Bristow, Naval Postgraduate School, for her help in processing data.

Finally, I would thank my wife, Colleen, and my three sons, Nathan, Kelin, and Tyler, for their love, patience, and understanding while achieving this degree.

I. INTRODUCTION

The nearshore bed on a barred beach is composed of complex bedforms due to varying wave and current regimes. Although there is abundant literature on small-scale morphology in rivers and estuaries induced by steady to quasi-steady flow regimes, few quantitative observations of bedforms are available for the nearshore. Corollary wave and current measurements are almost non-existent. The lack of data is due to difficulties in making measurements in the nearshore. Observations historically have been made by divers who are limited by visibility and the harsh nearshore environment, which can become unfavorable for observations even in the mildest of storms.

Small-scale morphology and bedforms were measured on a barred beach during the October phase of the DUCK94 experiment using a sonic altimeter and side-scan sonar mounted on the CRAB. Small-scale morphology is defined here as scales less than 5 m. Corollary measurements of waves and currents were made at the same time. The DUCK94 experiment was a pilot study and represented a first attempt to make quantitative, multi-scale measurements of nearshore morphology. During the three week phase of the experiment, the small-scale morphology varied significantly, both spatially and temporally, as wave and current climate varied during the passage of a major storm. Three separate sequences showing distinct differences in ripple characteristics and bedforms caused by varying wave and current processes are examined: mild waves and weak longshore current conditions resulting in wave ripples throughout the nearshore; storm waves with strong longshore currents resulting in lunate and straight-crested megaripples in the trough of the barred

beach; and narrow-banded, normally incident waves with a strong rip current resulting in a relatively planar bed everywhere except in the throat of the rip where megaripples were formed.

Several scales of ripples have been previously observed in the field; however, most measurements were limited to the smallest-scale, wave-induced ripples or vortex ripples and referred to here as wave ripples. Dingler and Inman (1976) used a moveable acoustic altimeter placed on a track on the bottom to profile the small-scale ripples outside the surf zone, but were limited to a single track of approximately 2 m in length. Other methods included using waxed combs shoved into the bed by divers to record ripple profiles. Miller and Komar (1980) found ripple wavelength to be related to the orbital diameter of the waves.

Wave ripples have been measured by numerous investigators in the laboratory. Nielsen (1981) summarized available laboratory data and found wave ripple length and height depended mainly on the mobility number, which is the ratio of the wave velocity magnitude to the sediment settling velocity. Southard et al. (1989) was able to obtain higher velocities and longer period waves in a water tunnel, and found the bed under pure oscillatory flow forms 2-D wave ripples under low velocity, short period (< 9 sec) waves, transitioning to 3-D ripples at higher velocity and longer periods, which suggested differing bedforms for higher velocities and longer periods. In the laboratory, longer period waves can only be achieved in water tunnels or prototype-scale wave tanks limiting superposed currents to collinear flow. In a laboratory basin, Van Rijn and Havinga (1995) observed ripple configurations under varying wave and current conditions. Two-dimensional ripples were

observed with only waves present, progressing to three-dimensional ripple patterns with strong currents acting. No significant change in ripple dimensions occurred due to a change in the angle between wave and current direction.

The least documented nearshore bedforms are intermediate scale megaripples owing to difficulties in obtaining quantitative measurements. The most visible evidence of mega-ripples is recorded in sedimentary deposits. Clifton et al. (1971) studied the internal structure of sediments obtained on a near-planar, high energy beach by trenching at spring low tide on the foreshore and coring offshore. Davis and Fox (1972), Davidson-Arnott and Greenwood (1976), and Hunter et al. (1979) similarly examined barred beaches. These observations are restricted to prograding beaches in which the sedimentary records are preserved. Hunter et al. (1979) found the dominant bedform in the outer, seaward region of the bar to be medium scale lunate megaripples facing in the direction of wave propagation. Restrictive diving conditions and planing off of the bar at high tides made observations on the bar difficult. When observed, bedforms on the bar crest were similar to those on the seaward slope of the bar. In the main part of the trough, longshore currents tended to remove finer sediments and generate traverse bedforms facing in the longshore direction. The most typical bedforms observed were slightly linguoid megaripples, linguoid to irregular ripples, and occasionally sand waves. In rip channels, which contain relatively finer sediments than does the longshore trough, the most common bedforms observed were seaward-facing lunate megaripples. (Hunter et al., 1979). Sherman et al. (1993) examined megaripple migration

and mixing depth in a rip-feeder channel. The results indicated the megaripple trough propagated approximately 1 m/hr.

A conceptual view of the small-scale morphology on a barred beach was summarized by Clifton (1976) based on diver observations (Fig. 1), which shows the transition of the small-scale morphology from wave ripples to megaripples on the seaward slope of the bar, to a planar bar crest due to the increase in wave intensity, and to wave ripples again in the trough where wave intensity decreased after waves crossed the bar. The observations are in agreement with the laboratory results of Southard et al. (1989), who observed the transition from 2-D to 3-D ripples with increasing velocities and longer wave periods.

The objective of this paper is to correlate small-scale morphology measured over a barred beach with waves and currents. In the following sections, a description of the DUCK94 experiment, the methodology of the data analysis, and the description of the small-scale morphology observed on Oct. 8, 12, and 20 are presented.

II. DUCK94 EXPERIMENT

The data presented here were obtained in the comprehensive nearshore DUCK94 experiment conducted in October 1994 at the U. S. Army Corps of Engineers Field Research Facility (FRF), Duck, North Carolina. The FRF is located on the Outer Banks, a barrier island formation. The FRF beach usually has a two-bar system which is composed of a dynamic inner bar (30-120 m offshore) and a secondary bar of lower amplitude (300-400 m offshore). The mean foreshore slope of the beach is approximately 0.08 (1:12) and the mean slope offshore of the bars is approximately 0.006 (1:170) (Lippman et al., 1993). The mean tidal range in the beach area is approximately 1 m.

Meteorological data of wind speed and direction, air and sea surface temperature, and atmospheric pressure were acquired simultaneously at two locations at the FRF. The weather during the October experiment was characterized by four distinct phases (Fig. 2): a "northeaster" with a front moving from north to south from 2-4 Oct.; moderate waves and weak currents and winds from the north 4-9 Oct.; relatively strong currents (0.5-1.0 m/s) and predominant winds and waves from the north associated with a second "northeaster" 10-17 Oct.; and variable currents and winds from the north and south 17-21 Oct.

The Coastal Research Amphibious Buggy (CRAB), an 11 m high, hydraulically driven, three-wheeled vehicle, is a uniquely stable platform from which to make measurements (Fig. 3). The primary purpose of the CRAB is to efficiently survey the bathymetry (order 3 cm rms vertical and horizontal accuracy) from the waters edge out to depths of 8 m in waves up to 2 m (Birkemeier and Mason, 1978). The surveys were

performed daily during the experiment by driving the CRAB in a series of cross-shore survey lines with its position tracked by a laser ranging/auto-tracking system approximately every meter. The alongshore separation of the survey lines was between 25 to 30 m. Using the CRAB, time encoded horizontal location and vertical relief of the bed for each survey line was obtained. Three-dimensional bathymetry mapped by the CRAB describing the large-scale morphology during the experiment are shown in Fig. 4.

The elevation of small-scale morphology was measured using a 1 MHZ sonic altimeter mounted on the CRAB 70 cm from the bed. The altimeter has a nominal sampling rate of 25 Hz and was time-coded with the bathymetry measurements. The sonic altimeter was used to measure the location of the bottom, with mm vertical resolution and accuracy of less than 2 cm, by measuring the travel time of an acoustic pulse from the altimeter to the bottom and back to the altimeter. The decrease in accuracy compared with resolution is due to the changing reflective surface resulting in a variability in the measured bottom elevation owing to the bed dialating or sediment transported along the bed as waves pass overhead. A theoretical sound speed is used to convert time into distance. An Automatic Gain Control (AGC) accommodates large fluctuations in acoustic properties of the water column, which improves the bottom-locating property of the altimeter. The transducer has an approximate 3.4 degree beam width which translates into a 4.2 cm footprint at 70 cm height from the bottom. The footprint may have a minor effect of height estimation and noise in the data for sloping bottoms due to sound arriving first from the uphill side of the footprint. Bubbles,

suspended sediments, and compactness of the bed are factors which may also contribute to scattered data points. (Gallagher et al., 1995)

The side-scan sonar depicts a high resolution plan view of the small-scale morphology. However, it does not directly measure amplitudes of the bedforms. The side-scan sonar operates at 500 KHz. This frequency is used to increase resolution due to the operating environment, which is in shallow depths. The sonar is suspended in the center of the CRAB approximately 1.25 m from the bed. The nominal horizontal range of the sonar was approximately 10 to 15 m to each side of the sonar, with exceptional ranges out to 25 m. Sonar ranges of 15 m allowed overlap of sonar data from adjacent survey lines, which gives a relatively complete view of the geometry and spatial representation of the ripple features. Bedform amplitude and geometry, bubbles, and suspended sediments all contributed to or limited increased sonar range and resolution. In this pilot experiment, the side-scan sonar output was recorded only on paper which does not allow rectifying the representation for range and speed of travel. The side-scan only records sonic reflections so that bedforms oriented normal to the sonic beam give the strongest reflections. The CRAB traversed the surf zone in lines perpendicular to the beach with the side-scan looking alongshore. Therefore, wave ripples parallel to the shore would not be expected to give strong sonic reflections and may not have been seen by the side-scan. This can make some of the side-scan interpretations difficult.

Corroborating wave and current data were acquired using an instrumented sled. A vertical stack of eight Marsh-McBirney two-component electromagnetic current meters with

2.5 cm diameter spherical probes were mounted on a 2.5 m mast to measure vertical profiles of the longshore current. The sled was oriented with the vertical stack of current meters placed on the up-current side to prevent the sled structure from contaminating flow measurements. Waves and mean water level were measured using an array of six pressure sensors configured on a 3 m square with one in the middle and another in the middle of a cross-shore leg. For data collection, the sled was first towed by the CRAB to its furthest position offshore, dependent upon wave conditions, for the first data run. A forklift on the beach pulled the sled shoreward approximately 10 to 30 m for each subsequent run. Data were collected at each location for approximately one hour at four to eight locations.

Additionally, directional wave spectra were acquired using a linear array of 10 pressure sensors in 8 m depth offshore of the survey area. A fixed current meter in the trough at line 820 m was used to acquire continuous longshore currents.

III. METHODOLOGY

The CRAB surveys and altimeter measurements were combined to obtain highly resolved bottom profiles. Bathymetry data measured by the CRAB were x, y, z (cross-shore, alongshore, and depth) locations and time. The sampling rate was approximately 1 Hz, although the data were not evenly spaced in time and often gapped by several seconds. The spatial separation of data is determined by how often the survey points are taken and is dependent on the speed of the CRAB. The nominal CRAB speed is O(1 m/s) resulting in a cross-shore resolution of O(1 m). The prism is located directly over the back wheels so that the response of the CRAB to changes in the bottom is directly measured. It is assumed the elevation error due to the tilt and roll of the CRAB owing to the bumpy bottom is small and can be neglected. Given the 8.3 m wheel base and 13.1 m height of the prism above the bed, 30 cm rms height bumps result in less than a 1 cm rms error.

High resolution bathymetry was measured using a 1 MHZ sonic altimeter mounted on the CRAB 70 cm above the bottom. The data acquired were time encoded distance from the altimeter to the bed. Since the altimeter was rigidly mounted on the CRAB, altimeter heights less than 70 cm indicate bumps or crests of ripples, whereas altimeter heights greater than 70 cm indicate holes or troughs of ripples. The altimeter had a nominal sampling rate of 25 Hz with variations up to +/-3 Hz. The altimeter has a much higher vertical resolution O(mm) than does the CRAB survey system. Depending on the CRAB speed, usually 0.5 to 1 m/s, the cross-shore resolution is on the order of 2 to 4 cm.

Spatial representation of the small-scale bathymetry was obtained by merging the CRAB survey and altimeter data by aligning the time series by linearly interpolating the CRAB survey data to the corresponding time of the altimeter data. From the alignment, profiles of cross-shore distance versus CRAB survey depth and height from the bed to the altimeter are obtained.

The altimeter data were generally noisy due to minor problems in the altimeter's logic of the AGC to track the bottom. The logic is designed to reject scatters and multiple bottom reflections. Noise was also introduced by strong scattering of the the acoustic pulses from bubbles entrained by wave breaking. Therefore, considerable effort was required to deglitch the data (Fig. 5). First, points above and below a certain band of acceptable altimeter heights were excluded. This resulted in a loss of only a very small number of data points for Oct. 8 and Oct. 20 when conditions were relatively mild. However, during stormy conditions such as on Oct. 12, wave breaking on the offshore bar filled the outer surf zone with persistent micro-bubbles, acting as strong sound scatterers, which resulted in the loss of altimeter data for 30 to 50 meters over the bar. For the times when the altimeter data was too noisy too be used, the altimeter data was set equal to 70 cm which inserted the CRAB survey depth.

A running median filter was next applied, which is particularly good at eliminating outliers in noisy data and can be applied to unevenly spaced data. The length of the filter varied between three and nine points, depending on the application. For example in the nine point filter, sequential points are sorted by increasing heights, and the mean of the three

middle values is assigned to the corresponding cross-shore distance. This filtering process removes stray data points while retaining a smoothed altimeter height profile (Fig. 5). An expanded view of the filtered altimeter data is presented in Fig. 6.

The effects of applying the median filters to the altimeter data are examined by calculating empirical response functions for various filter lengths as the ratio of spectra for filtered and unfiltered data. Data acquired on Oct. 8, when the shortest wavelength wave ripples were present during the experiment, are used as a worst case. A 110 m cross-shore distance is used where the altimeter data was relatively homogenous. To calculate the wavenumber spectra and rms roughness of the bed, unevenly spaced data are linearly interpolated to evenly spaced 2 cm increments of the cross-shore distance. The spectrum of a 20 m section is determined and then incremented by 10 m in the cross-shore direction giving 50 percent overlap. In calculating the spectra, a 10 percent cosine-taper window is applied to the data. The individual spectra are then averaged. This method was performed on data filtered by a nine, five, and three point running median filter and on raw data not filtered. The three point running mean filter sorts three points by increasing height and plots the middle value with the corresponding distance. This filter effectively removed outliers but still retained the characteristics of the unfiltered data. All four spectra show peaks at the same wavenumber, however, the amplitudes of the spectral peaks for the nine and five point filtered data are reduced with increasing wavenumber. Empirical transfer functions are calculated from the ratios of filter spectra with the raw spectrum. The median filter has a nonlinear spectral response function because the averaging length can vary, i.e., from

adjacent points somewhere within the nine points, to three points including the extremals at the first and last points. Since the filter averages three points, it would be expected to have similar characteristics to a running mean filter whose spectral transfer function is given by

$$H(k) = \frac{\sin(\pi k n \Delta x)}{\pi k n \Delta x} \qquad (1)$$

where Δx is the sampling distance and $n\Delta x$ is the distance averaged over (in this example $n\Delta x$ varies between $3\Delta x$ and $9\Delta x$). The magnitudes of the empirical transfer functions are compared with running mean transfer functions using several values of $n\Delta x$ ranging from 6 to 36 cm in (eqn. 1). The comparison suggests the averaging lengths of 6 cm and 30 cm best fit the three and nine point filtered transfer function plots (Fig. 7).

The response of the CRAB to the small scale variations is dependent on the bearing capacity of the bed and the wheel diameter (2 m). To determine the scale of the ripples which are filtered by the CRAB, a similar method was used as in the testing of the running mean filters. Sections of three cross-shore profiles were selected from Oct. 10, 12, 20 in which the sections showed large bedform elevation variability with each section approximately 60-100m in length. The large, low frequency, macro-profile variations were removed by subtracting a third-order polynomial best fit curve to 20 m cross-shore lengths of the combined CRAB survey and altimeter profile and the CRAB survey profile by itself. Wavenumber spectra were calculated for the 20 m lengths and were incremented by 5 m for the length of section. The spectra were averaged and an empirical response function is

calculated from the ratio of the averaged CRAB profile spectra with the combined CRAB and altimeter profile spectra (Fig. 8). Assuming the effect of a tire rolling over the bottom responds similar to a running mean average filter, eq. 1 was applied using various $n\Delta x$ values. The empirical CRAB response function values are less than predicted by the running mean filter at low frequencies because of subtracting out the low frequencies using the polynomial fit to the data. The results suggest the CRAB responds to the larger features, but filters features less than 1-2 m.

A source of noise found throughout the altimeter data was due to wave crests hitting the CRAB causing fluctuations in the altimeter data of up to 2 cm, depending on the wave height. The speed of the CRAB and period of the waves determined the spatial scale of the wave interaction. A clear example is provided on the 20th during a time of narrow banded 14 sec swell when the CRAB was driving over a very smooth bottom (Fig. 9). The mean CRAB speed of 0.8 m/s interacting with the narrow banded 14 sec waves resulted in an apparent 1-2 cm bump approximately every 10 m. It is not known if the bump is caused by the wave lifting the CRAB or the bed being dialated under the crest of the wave. This information is later used when interpreting wavenumber spectra to determine false ripple wavelengths.

IV. OCTOBER 8 MORPHOLOGY

The large-scale morphology on Oct. 8 at first glance appears to be relatively homogeneous. The offshore bar is nearly parallel to the shore and is located approximately 230-250 m offshore (Fig. 4). Therefore, it would be expected the small-scale morphology would also be homogenous alongshore throughout the survey area given the same wave and current conditions. The small-scale morphology observed in the side-scan is generally characterized by crossing wave ripples from two directions. Ripples are observed from the foreshore to offshore of the bar for the entire survey area. However, close examination shows that the small-scale morphology is not homogeneous and that ripple patterns vary both in the cross-shore and alongshore directions.

A northeaster passed through the area on Oct. 3 resulting in maximum winds from the northeast at 16 m/s with significant wave heights reaching 2.3 m and peak periods of about 6-7 sec (Fig. 2). Strong longshore currents to the south were also observed. A period of mild wave and weather conditions followed between Oct. 4-9. The waves on Oct. 8 were short period (4 sec.) and approximately 5 to 10 degrees from the north. Significant wave heights were on the order of 0.5 m. Longshore currents were weak and from the north. The large-scale morphology of the survey area did not change throughout the period Oct. 2-9. Wave and current conditions of the 8th are not expected to form crossing wave ripples from two directions.

Two representative lines (940 and 710) of cross-shore combined CRAB and altimeter profiles are selected to depict the differences present in the small-scale morphology for the survey area (Figs. 10 and 11, lower panels). South of line 860, the small-scale morphology was due to wave ripples and is characterized by line 710. To the north, the small-scale morphology in the trough and on the seaward slope of the bar was primarily due to megaripples and is characterized by line 940. The primary differences in the ripple dimensions between the two representative lines are observed in the trough and the seaward slope of the bar. The trough extends from the foreshore to the crest of the bar (150 to 240 m). The seaward slope of the bar area extends from the crest of the bar and seaward 60 m (240 to 300 m).

To obtain a general idea of the wavelengths of the small-scale morphology, average spectra were calculated for the trough region and the seaward slope of the bar region. A third order polynomial fit is subtracted from the combined CRAB and altimeter data, and then filtered using a three point running median filter. The spectra are calculated for 20 m cross-shore segments incrementing by 5 m to give a 75 percent overlap. The average of the individual spectra for each region is then obtained for each line. An example of averaged spectra for the trough region and seaward slope of the bar region is shown in Fig. 12. The spectra tended to be broad, which indicates that more than one wavelength is present in the spectra. Some (unknown) amount of broadening can also be due to ripples from different directions.

The small-scale morphology in general showed large variation in the cross-shore; as a consequence, the condition of spatial homogeneity (stationarity) required for calculating averaged spectra is not met. Therefore, continuous wavenumber spectra are calculated for 20 m cross-shore segments at increments of 1 m across the surf zone. The spectra are summed over three wavelength bands (0.4-0.83 m, 0.83-1.67 m, and 1.67-5 m) plus the total band (0.4-5m), resulting in 16, 34, 52, and 102 degrees of freedom for each band respectively. The rms height of each band is calculated as the square root of the variance within each band (Figs. 10 and 11). The wavelength bands were selected based upon examination of many averaged spectra (e.g. Fig. 12). It is pointed out that variances sum, not rms heights, such that the rms height of the sum of the three bands is calculated from the square root of the sum of their variances.

As the small-scale morphology is defined as having scales less than 5 m, variance contributions for wavelengths greater than 5 m are not included in the rms calculations. The spectra often showed a dominant contribution at wavelengths greater than 5 m (e.g. Fig. 12, upper panel). Contributions at scales greater than 5 m are due to contributions by the macro-scale morphology not being completely subtracted out using the best fit polynomial over the 20 m section, and possible noise contribution due to the waves hitting the CRAB.

The small-scale morphology in the trough of line 940 is predominantly long wavelength megaripples (1.67-5 m), which are superimposed by shorter wavelength wave ripples. The trough region of line 710 has a more homogeneous ripple pattern in which no wavelength band is predominates. The seaward slope of the bar of line 940 shows the ripple

wavelength bands of 0.83-1.67 m and 1.67-5 m are dominant and the rms height is on the order of 3 cm. Line 710 for the same area again shows a relatively homogeneous ripple wavelengths with rms heights of approximately 2 cm.

The rms elevation, σ, can be related to the crest to trough heights of the ripples assuming the ripple elevations are Gaussian distributed and the wavenumber spectra are reasonably narrow banded such that the ripples heights are Rayleigh distributed. For Rayleigh distributed heights, the significant ripple height, $r_s = 4\sigma$ and the maximum ripple height, $r_m = 8\sigma$. These approximations agree qualitatively with the observations.

The CRAB and sonic altimeter data can only observe the small-scale morphology directly below. The side-scan sonar can observe the small-scale morphology to approximately 10-15 m on either side of the side-scan and therefore aids in a better interpretation of the bedforms present. The side-scan sonar plots of lines 940 and 710 can be used to correct the calculated wavelengths acquired from the single altimeter data (Fig. 13). The side-scan plot of line 940 shows relatively straight crested ripples with wavelengths of approximately 50 cm crossing at a 30-40 degree angle relative to the shoreline, from the southeast, out to the bar. The corrected wavelength is calculated $L = \lambda\cos(90 - \alpha)$, where λ is the measured wavelength in a line perpendicular to shore, and α is the angle to shoreline. Seaward of the bar, the side-scan sonar observed crossing wave ripples from two directions. The measured ripple wavelengths of greater than 0.83 m were not obvious in the side-scan. For line 710, the side-scan observed the crossing wave ripple pattern for the length of the survey line, with the dominant pattern again from the southeast. The ripple wavelength

observed on the side-scan plots was generally on the order of 0.5-1.0 m. Surprisingly, the dominant crossing wave ripples observed by the side-scan is only a small contribution to the small-scale morphology variance. This may indicate the larger, lower wavenumber contributions to the variance were long crested ripples perpendicular to shore resulting in low sonic reflection in the side-scan sonar.

V. OCTOBER 12 MORPHOLOGY

The large-scale morphology of Oct. 12 is similar to that of Oct. 8. The offshore bar is nearly parallel to the beach, but migrated 30 m offshore to approximately 260-280 m offshore (Fig. 4). Although the large-scale morphology is relatively the same for the two days, the small-scale morphology is significantly different due to differences in the wave and current processes. Large amplitude megaripples are now present in the trough and no regular bedform patterns are observed seaward of the bar for the entire survey area.

The dramatic differences in the wave and current parameters for the two days is the result of a second storm which arrived in the area on Oct. 10. On Oct. 9, wave direction was approximately 30 degrees from the south with the period of the waves being approximately 6-7 sec. Waveheights were on the order of 0.5 m and the longshore currents were weak and variable. As the storm arrived, wave direction shifted to 10 degrees from the north with a period of 6 sec. Waveheights increased to 2 m and the longshore currents increased to 0.5-1.0 m/s to the south. The strong longshore current which appeared on the 10th is believed to be the dominant process which formed the small-scale morphology present in the trough on the 12th.

The small-scale morphology across the surf zone is relatively homogeneous alongshore and therefore, the survey area is represented by the combined CRAB and altimeter profile of line 940 (Fig. 14, lower panel). Detailed current data on line 940 were acquired several days prior to and including the 12th, which is useful in describing the temporal evolution of the small-scale morphology. The small-scale morphology in the

trough compared with the region seaward of the bar crest are distinctly different. Altimeter data for profile is not available from 210-260 m due to waves breaking on the bar. The CRAB survey data is inserted into the profile and therefore the bottom is not as highly resolved in this area as it is elsewhere.

Wavenumber spectra are calculated for line 940 for incremented 20 m sections summed over the three same wavenumber bands (Fig. 14, upper panel) in the same manner as for Oct. 8. The small-scale morphology rms roughness was approximately 3-5 cm in the trough region on the 10th at the onset of the longshore current. The rms roughness of the 12th shows a distinct increase of the rms roughness in the trough as the megaripples continued to evolve. The rms roughness is primarily associated with the larger ripple wavelengths of 1.67-5 m across the survey line. Ripple wavelengths of 0.4-0.83 m and 0.83-1.67 m are significant out to approximately 200 m, but due to the lack of altimeter data from 210-260 m, the smaller wavelengths are not resolved. Seaward of the crest of the bar, the bed is void of any small-scale variations.

The side-scan sonar observed a sinuous ripple pattern at and nearly parallel to the beach (Fig. 15). The ripple patterns were only observable in the inner trough for the survey area because of bubbles due to breaking waves on the bar degrading side-scan performance. Ripple wavelengths observed from the side-scan were in the 1 m range. Ripple with wavelengths larger or smaller than 1 m were not observed. Ripple patterns were also measured using a rotating side-scan sonar mounted on the sled, which showed the megaripples in the surf zone to be lunate, facing in the direction of the longshore current.

VI. OCTOBER 20 MORPHOLOGY

The macro-morphology in the survey area on the 20th shows a dramatic hole in the inner bar as a result of a rip current (Fig. 4). The small-scale morphology is characterized by two distinctly different areas of large megaripples in the throat of the rip current with the area outside the rip devoid of ripples.

The rip current observed in the survey area on Oct. 20 started to develop on Oct. 14. The large scale morphology on Oct. 14 is similar to Oct.12 (Fig. 4), and is characterized as having straight and parallel contours with an offshore bar approximately 240 m offshore. The storm which started to propagate through the area on the 10th progressed offshore and stalled. With lengthening duration of winds, wave heights increased from 1.6 m on the 14th to a maximum of 4 m on the 15th and then tapered off to 1.5 m on the 20th. Waves throughout this period were near normally incident (within 6 degrees from the north or south) and narrow banded, with the peak period increasing from approximately 8 sec. on the 14th to 13.5 sec. on the 20th (Fig. 2). Normally incident waves are good conditions for rip currents to occur, as any alongshore perturbation can cause variable wave heights alongshore, resulting in variable set-up alongshore. The variable alongshore set-up generates hydrodynamic pressure gradients, which are relieved by rip currents flowing offshore. Longshore currents, as measured from the fixed current meter at line 820, were relatively weak and variable on the 14th and less than 0.5 m/s to the north on the 20th, which appear to be feeder currents to the rip.

Observation of the temporal evolution of the large- scale morphology is limited due to the CRAB not being able to operate during the height of the storm on the 15th and being limited to the area inside the bar on the 14th, 16th, and 17th due to large waves. The most striking observation is the hole in the bar with the bar bowed seaward due to the rip current. The bar is parallel to the beach and is located approximately 210-225 m offshore north of the rip area, shifting to greater than 300 m offshore in the rip area. The narrow trough, north of the rip area, acts as a rip-feeder channel and has the same small-scale morphological features as the rip area.

The dominant small-scale morphology observed in the rip area are seaward facing lunate and straight-crested megaripples. The area immediately north and south of the rip current is void of any discernable small-scale morphology with the exception of the rip-feeder channel. Representative small-scale morphology in the throat of the rip current (line 1030) and the area away from the rip current (line 785) are shown (Figs. 16 and 17) for the combined CRAB and altimeter survey profiles. The features evident in the survey lines can be further examined by calculating rms roughness and wavenumber spectra.

Wavenumber spectra are calculated for incremented 20 m cross-shore sections of lines 1030 and 785 and summed over three wavelength bands (Figs. 16 and 17). The rms height of each wavelength band is again calculated as described for Oct. 8. Typical rms roughness values in the rip area range from 5 to 15 cm, which are an order of magnitude larger than rms roughness values away from the rip. A contour plot of rms roughness values for the survey area is shown in Fig. 18, which displays the extreme variability of roughness

in the rip current area compared with that of the area away from the rip current. The rip current, as qualitatively observed with dye, is superimposed on the accompanying contour plot of the macro-scale bathymetry. The region of maximum rms roughness in the rip area is in the trough, extending from the foreshore (200 m) to the offshore bar (300 m). The average rms roughness for the representative line in the throat of the rip was 5 to 8 cm. The bed is essentially smooth away from the rip current with rms roughness values being less than 2 cm, which appears to be the result of planing action of the long period swell.

In the throat of the rip, the rms height associated with wavelength bands of 0.4-0.83 m, 0.83-1.67 m, and 1.67-5 m all appear to be significant. This implies that several scales of ripples are present. The side-scan plot encompasses lines 1030 and 980, which are in the throat of the rip and approximately 20 m to either side (Fig. 19). The extent of the plot in the cross-shore direction is from approximately 195-285 m, with the area indicated by the box in Fig. 18. From the side-scan plots, lunate and straight crested megaripples are observed. The wavelength of the ripples as measured from the side-scan plots is approximately 1-2 m. Observations of the ripples suggest the rip flowed in a southeast direction which is shown by the ripple patterns south of line 1030.

VII. DISCUSSION

Nielsen (1981) summarized the results of wave ripple measurements in the field, relating wave ripple height to the mobility number, ψ

$$\frac{\eta}{a} = 21\psi^{-1.85} \quad ; \quad \psi > 10 \tag{2}$$

and ripple wavelength to mobility number

$$\frac{\lambda}{a} = \exp\left(\frac{693 - 0.37\ln^7\psi}{1000 + 0.75\ln^8\psi}\right) \tag{3}$$

where mobility number is defined as the ratio of the drag force by the wave velocity to the force of gravity on the sediments

$$\psi = \frac{(a\omega)^2}{(s-1)gd} \tag{4}$$

and s is the specific gravity of quartz sand, d is the sand grain diameter and ω is the radial wave frequency. The excursion amplitude of the waves at the bottom, a, is calculated from linear wave theory

$$a = \frac{H_s}{\sqrt{2}\sinh Kh} \tag{5}$$

where H_s is significant wave height, K is wavenumber, and h is depth. Wavenumber is

related to radial wave frequency using the dispersion relationship from linear wave theory, $\omega^2 = gK\tanh Kh$.

Hourly values of H_s at various locations across the surf zone were calculated for 2-20 October using the model of Thornton and Guza (1983) with input of hourly averaged wave height, peak frequency and mean direction measured at the 8m array (given in Fig. 2), along with hourly tide elevation, and bathymetry measured each day. The model has two free parameters, β and γ, corresponding to the intensity of wave breaking and the percent of breaking waves. The model parameters were calibrated using H_s values measured at various locations within the surf zone using a pressure sensor mounted on the sled for Oct. 8, 10, 11, 12, and 20. One hour pressure record sprectra were calculated and converted to wave surface elevation spectra using the linear wave theory transfer function. H_s was calculated as $H_s=4\Lambda$, where Λ is the standard deviation of the wave band of frequencies (0.05-.5 Hz). The optimized parameters were $\beta = 1.0$ and $\gamma = 0.4$. The errors between the predicted and measured H_s values were less than 15 percent, which is sufficiently accurate for the application here. Hourly values of η and λ based on calculated ψ values were calculated using the predicted H_s values (Fig. 20), which are used to compare with the measured ripple rms roughness and ripple wavelengths. Values are calculated for in the trough, on top of the bar, and offshore the bar. The twice daily oscillations in the predicted values are due to depth variation of the tide. For values of ψ greater than 200, eq. 2 predicts the ripples are essentially planed off by the waves. It is assumed in comparing the measured rms roughness, σ, with the predicted peak to peak ripple heights, η, $r_s = 4\sigma \sim \eta$.

On Oct. 8, the ripple dimensions in the 0.4 to 0.83 m wavelength band were reasonably predicted in the trough. Equation 2 overpredicted the ripple heights offshore and on top of the bar. The ripples and megaripples of longer wavelengths were not predicted. This suggests that the megaripples on line 910 were residual from some earlier time of formation and processes, such as on Oct. 3 when a strong longshore current was present. The crossing ripple patterns observed may have been the result of the bimodal pattern of the wave direction from Oct. 5-7, in which the waves were propagating from both the north and south directions or from the earlier storm.

On the 12th, during a time of moderate storm waves, the small-scale morphology of the trough region is characterized by megaripples which are superimposed by smaller wavelength ripples, O(1 m). The predicted ripple heights are planed off across this profile based on the large ψ values. The measured ripples offshore of the bar were planar as predicted. However, the measured ripple heights within the trough were significant. On top of the bar, the altimeter did not work because of bubbles, so a comparison can not be made. The longshore current was relatively strong as shown by the longshore current profiles (Fig. 14). The waves and currents in the trough region are nearly perpendicular. Amos et al. (1988) found that when waves superimposed with perpendicular or near-perpendicular currents, two ripple systems may coexist with one or the other being better developed according to the relative strength of the current.

The small-scale morphology measured in the trough are similar to the observations of Hunter et al. (1979) in the trough region of a barred beach during a time when moderate

longshore currents were measured. Hunter et al. observed seaward-facing lunate ripples at the toe of the beach and long-crested ripples seaward of the lunate ripples. They also observed, at times, the longshore facing ripples developed in response to longshore flow either parallel or perpendicular to the main longshore current.

On the 20th, the calculated mobility number is large across the surf zone predicting a planar bed everywhere. The prediction is in agreement with the measurements outside the rip area. However, since in the rip area the megaripples had amplitudes of 10 to 40 cm with wavelengths varying from 1 to 2 m, it is inferred that the megaripples were formed as a result of the rip current, which dominated over wave processes in the rip area. The megaripples were generally asymmetric with the steep slope facing seaward indicating the ripples were formed primarily as a result of the rip current. However, some ripples were symmetric while others were asymmetric facing toward the beach which may infer a more complex formation due to a combination current and wave interactions.

VIII. CONCLUSIONS

Quantitative measurements of small-scale morphology on a barred beach were acquired during the DUCK94 experiment. The measurements were made using a sonic altimeter and a side-scan sonar mounted on the CRAB. Corollary wave and current measurements were made using an instrumented sled and fixed pressure sensors and a current meter. Three separate sequences are examined in which distinctly different ripple dimensions and bedform types were observed owing to varying wave and current regimes.

A qualitative conceptual model for small-scale morphology on a barred beach from Clifton (1976) is used as a framework for comparison. Clifton's model assumes that the beach is homogeneous in the alongshore direction, and thus does not apply to the rip channel observed on Oct 20.

The measurements of small-scale morphology on Oct. 8, when mild waves and weak longshore currents prevailed, are generally in agreement with the observations of Clifton (1976). Clifton identified wave ripples transitioning to megaripples on the seaward slope of the bar, a planar bed on the bar crest, and wave ripples in the trough. This model both compares and contrasts with the observations of lines 940 and 710. Observations of line 940 indicate megaripples are present in the trough and on the seaward slope of the bar. Ripples are also present on the bar crest, although the rms height is relatively smaller. Observations of line 710 show a relatively homogenous wave ripple pattern across the surf zone with no megaripples present.

Oct. 12 is characterized by the occurrence of a strong longshore current. The small-scale morphology of the inner trough region is characterized by relatively straight-crested megaripples (1.67-5 m) generated by the longshore current, superimposed by smaller wavelength ripples O(1 m), which is different from Clifton's model. Seaward of the bar, the bed was essentially void of ripples.

Oct. 20 is characterized by a rip current with two distinct areas of small-scale morphology. In the throat of the rip current, straight-crested and lunate megaripples were observed and had amplitudes of 10-40 cm with wavelengths of 1-2 m. The area away from the rip current was void of any ripple patterns as a result of the planing action of the long period swell.

Wave ripple height and wavelength were calculated using predictive equations by Nielsen (1981) at locations within the trough, on the bar, and offshore. The ripple dimensions in the trough region on Oct. 8 were reasonably predicted, as wave processes were dominant. The equations, however, did not predict the megaripples present in the trough or seaward slope of the bar in the northern part of the survey area. Megaripples were observed in the current-dominated regions of the nearshore for Oct. 12 and 20 and, therefore, Nielsen's equations are not expected to predict these features. The equations were able to predict the lack of ripples observed away from the current-dominated regions on the 20th.

The wavenumber spectral results infer a spatial and temporal variability of ripple dimensions in both the cross-shore and alongshore directions. The wavenumber spectra were generally broad, indicating that several ripple wavelengths coexisted as a result of newly

formed ripples combined possibly with residual ripples from the past to form a complex series of ripple patterns.

The DUCK94 experiment was a pilot study which represented a first attempt to make quantitative, multi-scale measurements of nearshore morphology. Results of the data acquired during the experiment indicate that reliable, quantitative measurements of small-scale morphology are obtainable using acoustic methods, even during storms and in rip currents.

In the upcoming Sandy Duck experiment, to be conducted in 1997 at the same beach, a 5 m linear array of seven altimeters will be mounted across the back of the CRAB. A digital recording, 500 kHz side-scan sonar will also be mounted on the CRAB. The array of altimeters will allow calculating 2-D directional spectra of the small-scale morphology to obtain robust height and direction statistics. The digital side-scan will allow enhancement, rectification, and mosaicing of the images.

APPENDIX

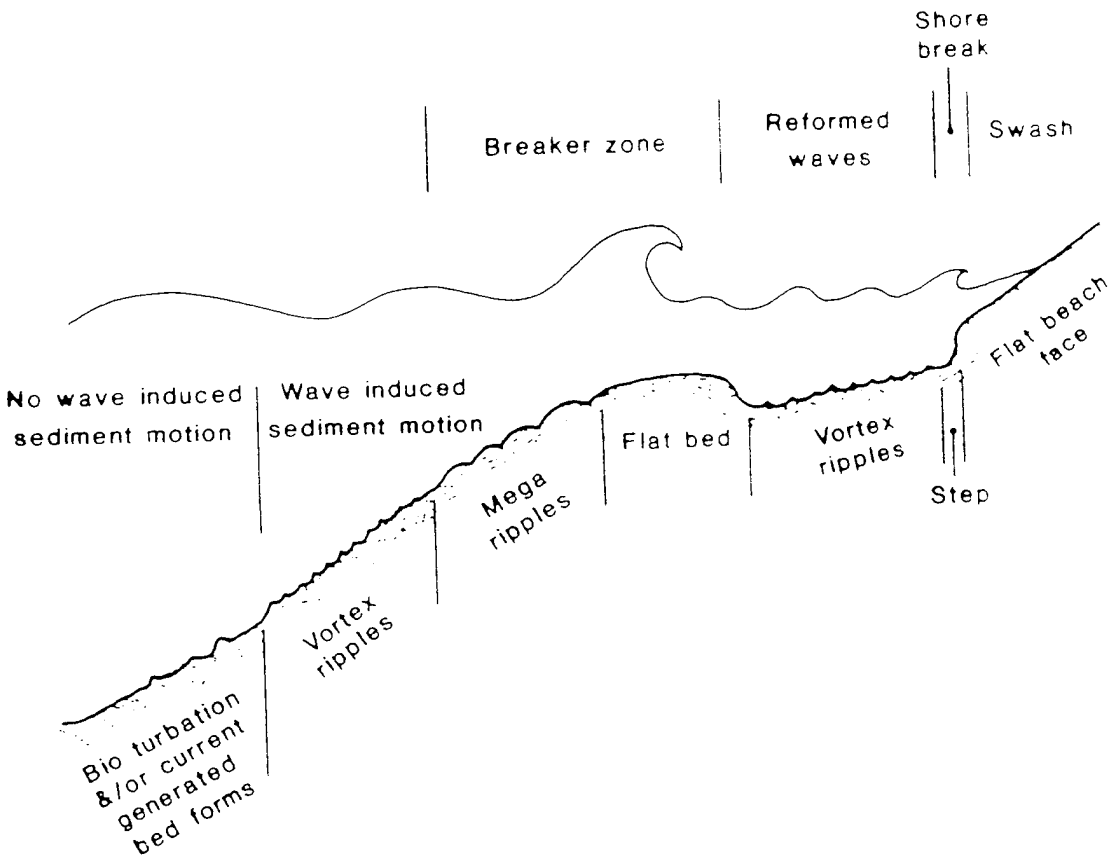

Figure 1. Conceptual model of small-scale morphology observed on a barred beach (from Clifton, 1976).

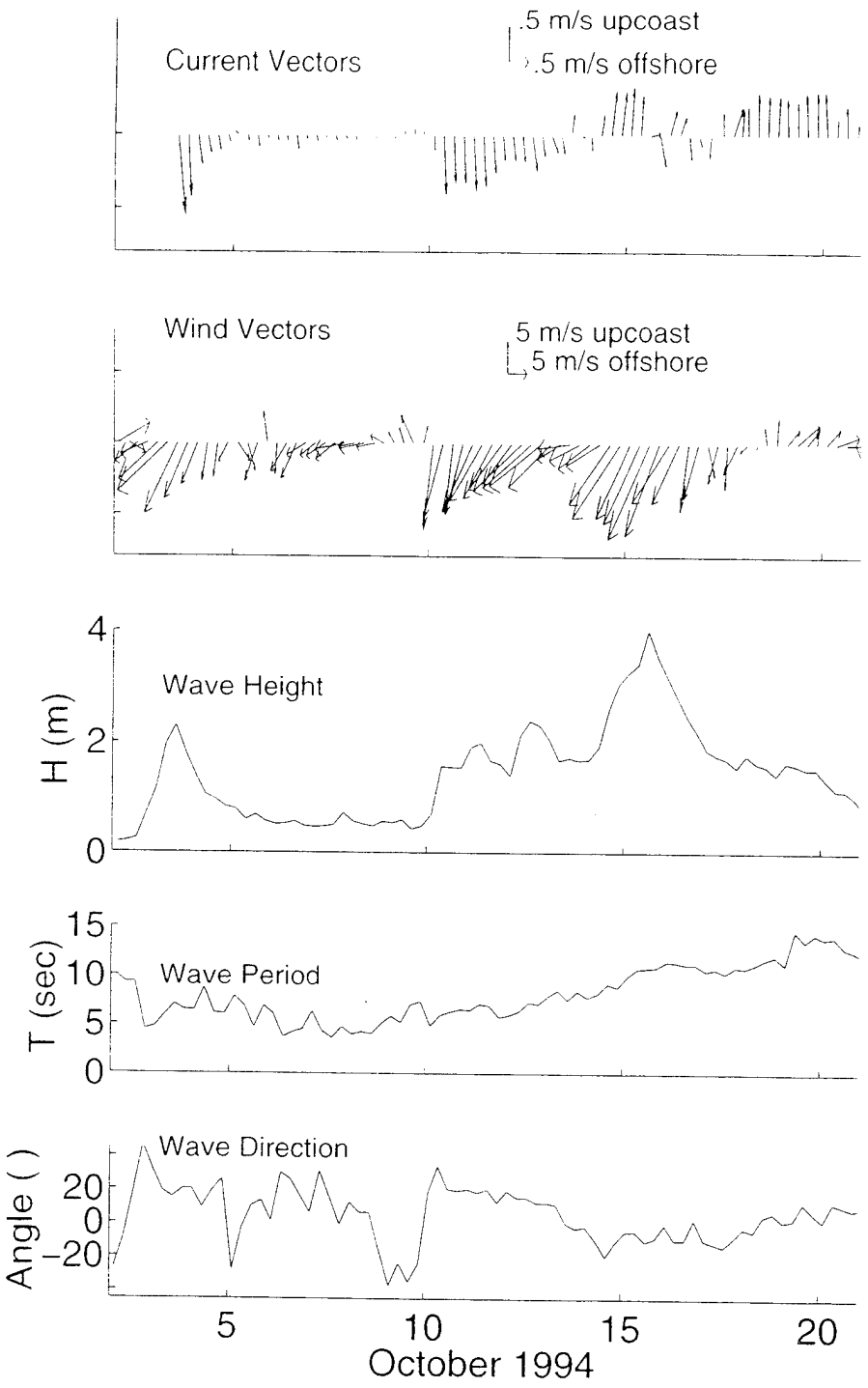

Figure 2. Climatology during the October phase of the DUCK94 experiment. Currents were measured from the middle of the trough. H is significant wave height and T is the period of the peak frequency measured in 8 m depth.

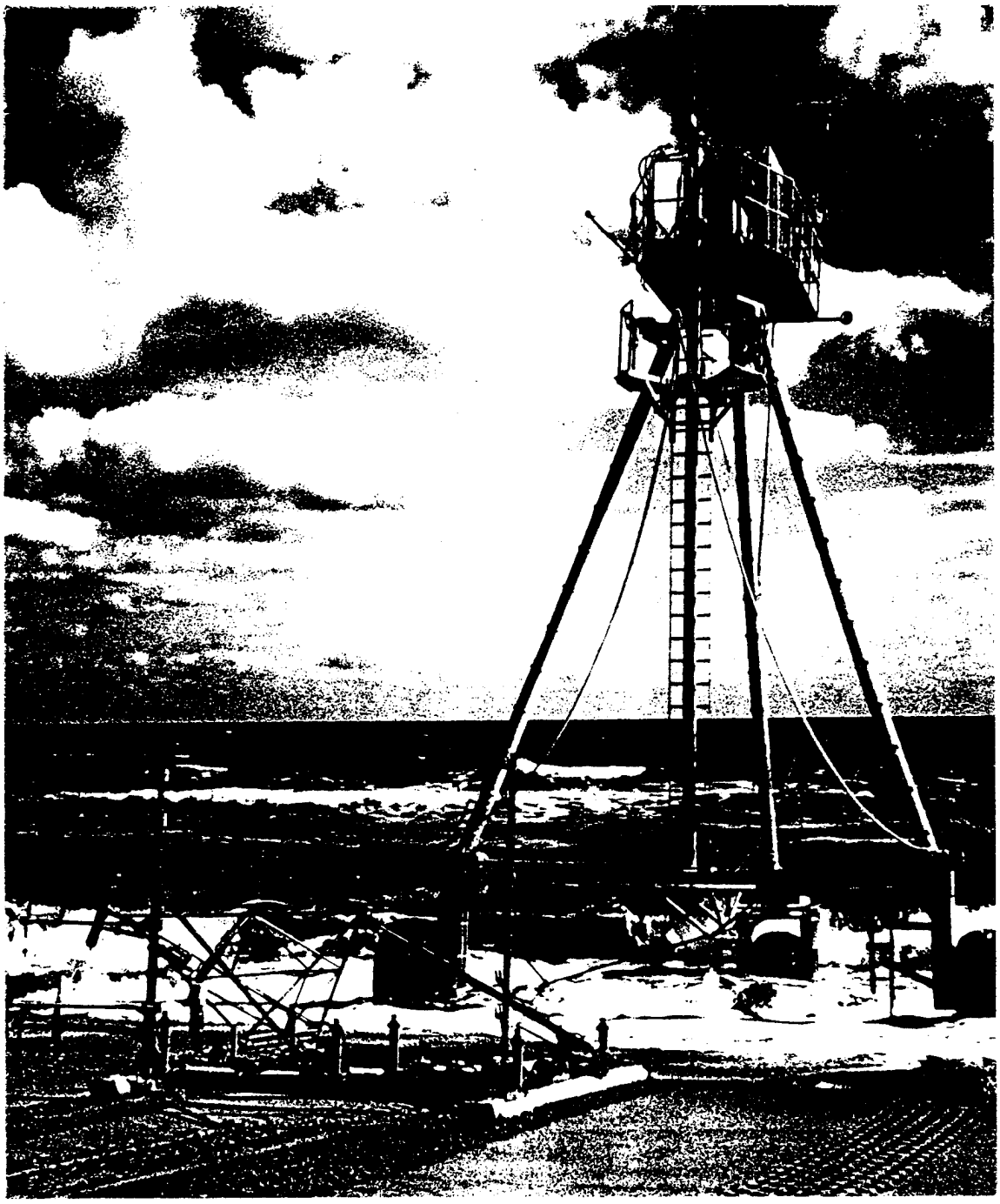

Figure 3. CRAB and instrumented sled on the beach during the DUCK94 experiment.

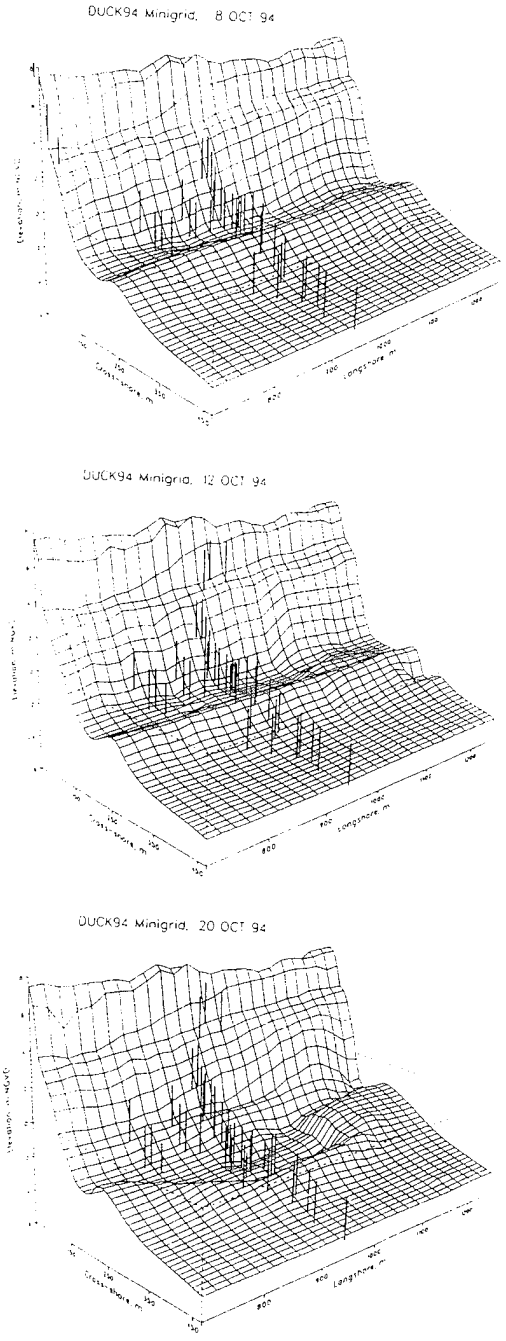

Figure 4. Three-dimensional bathymetry profiles of the survey area as mapped by the CRAB for the three days considered (Oct. 8, 12, 20).

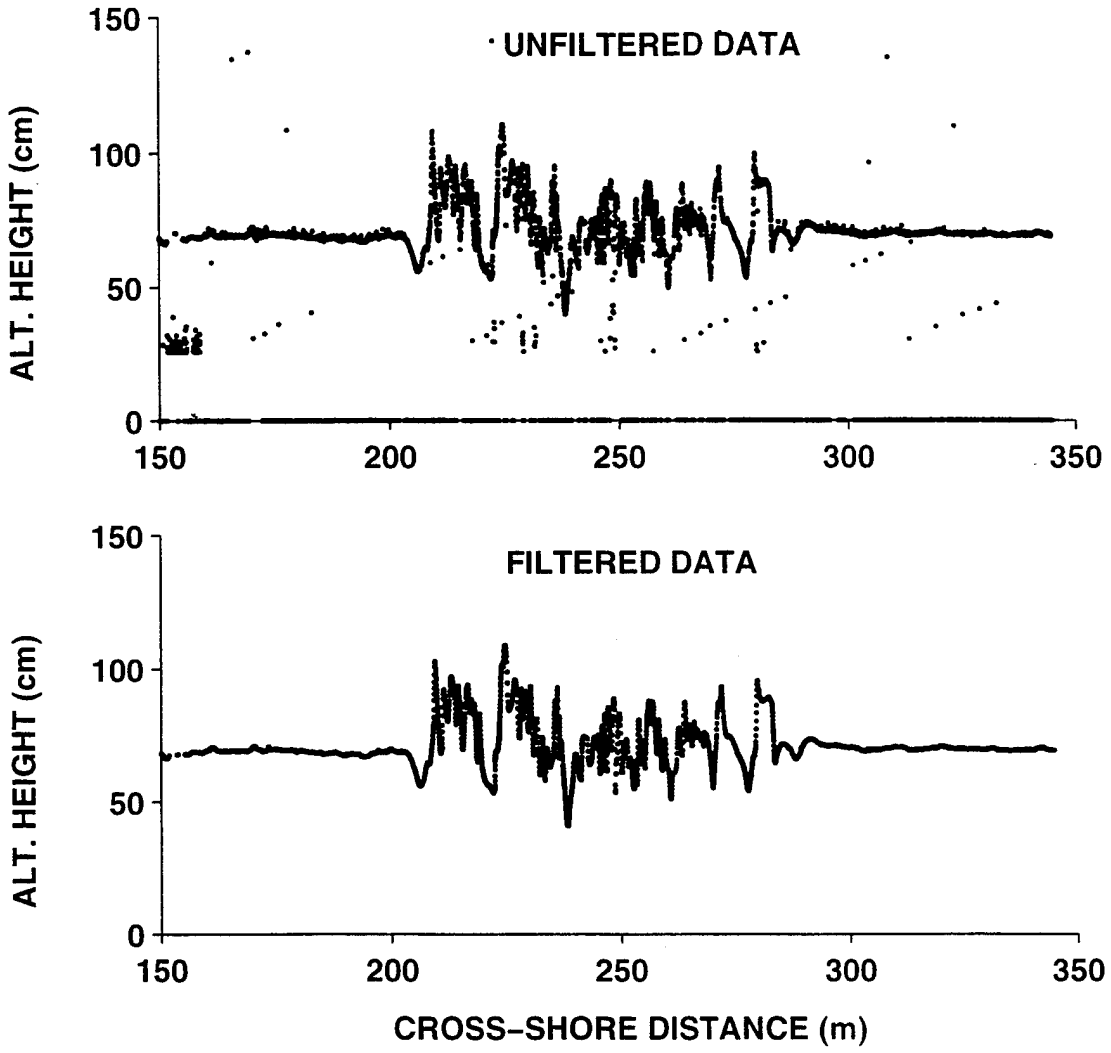

Figure 5. Example of unfiltered altimeter data (upper panel) and the filtered altimeter data after applying a nine point running median filter (lowere panel) for Oct. 20, line 1030.

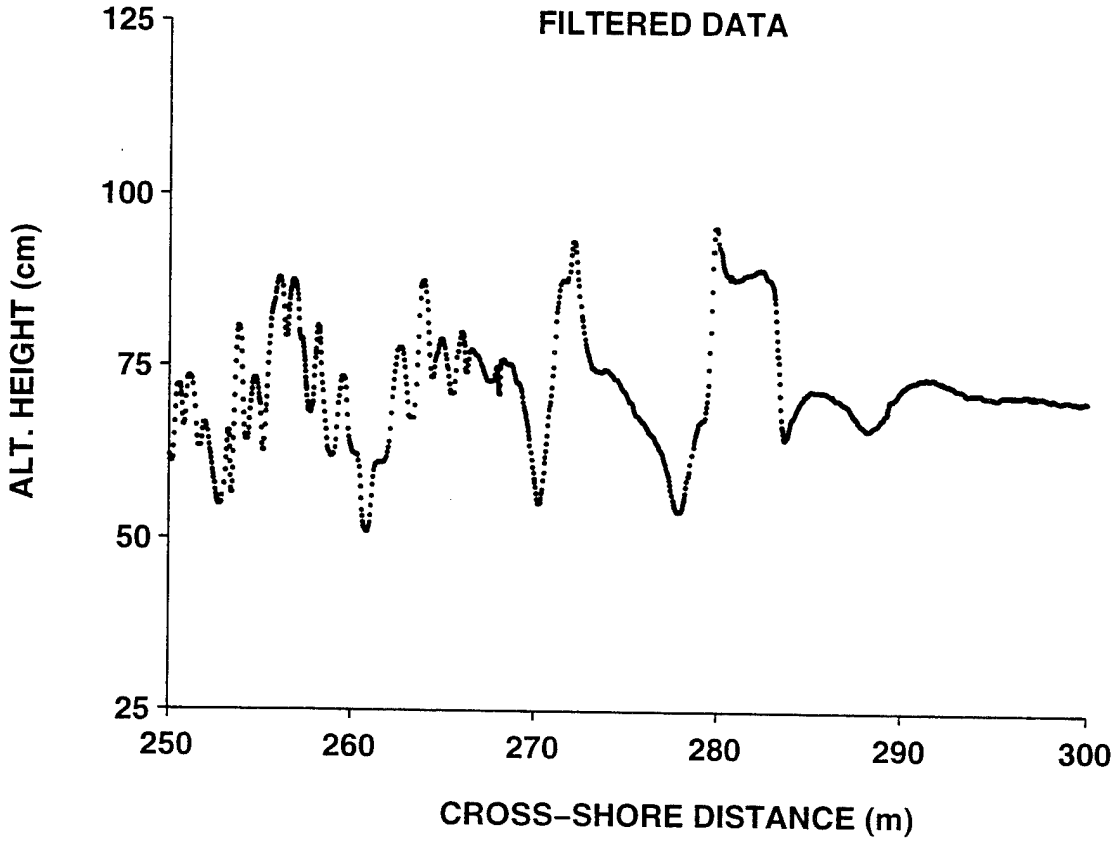

Figure 6. Expanded section of filtered altimeter data for Oct. 20, line 1030.

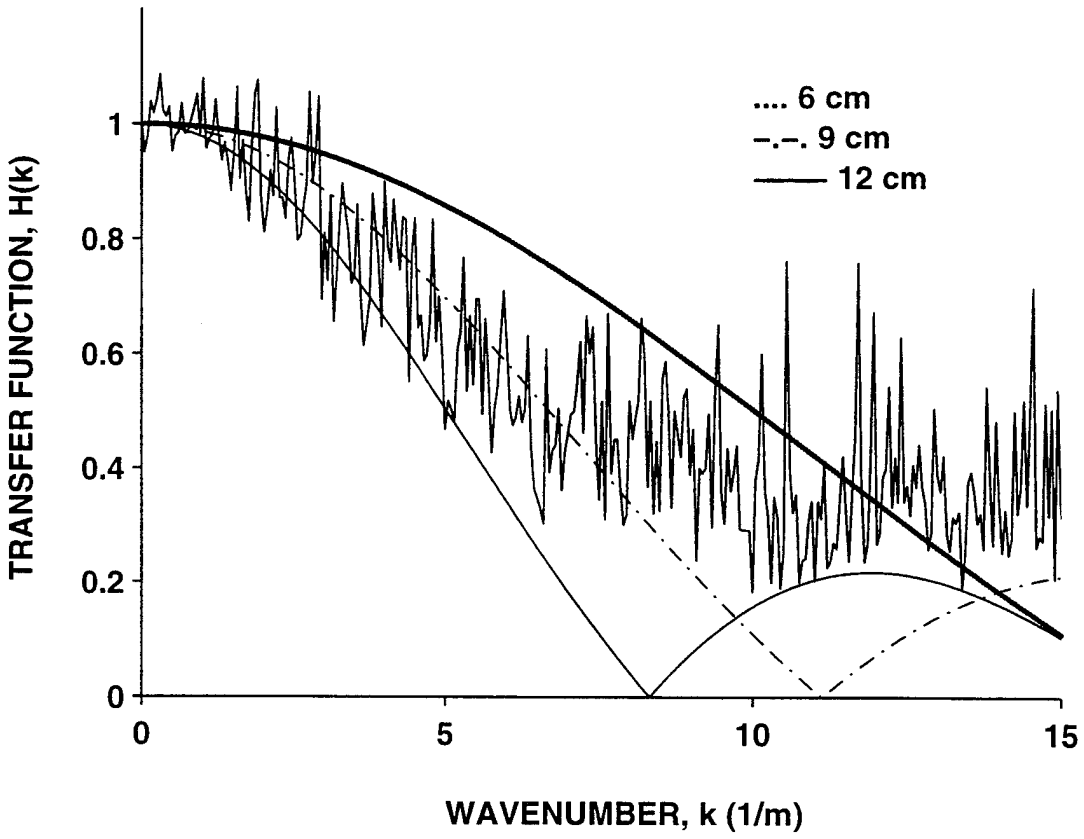

Figure 7. (a) Empirical transfer function of a three point running median filter calculated using altimeter data compared with the spectral transfer functions of a running mean filter with varying averaging lengths.

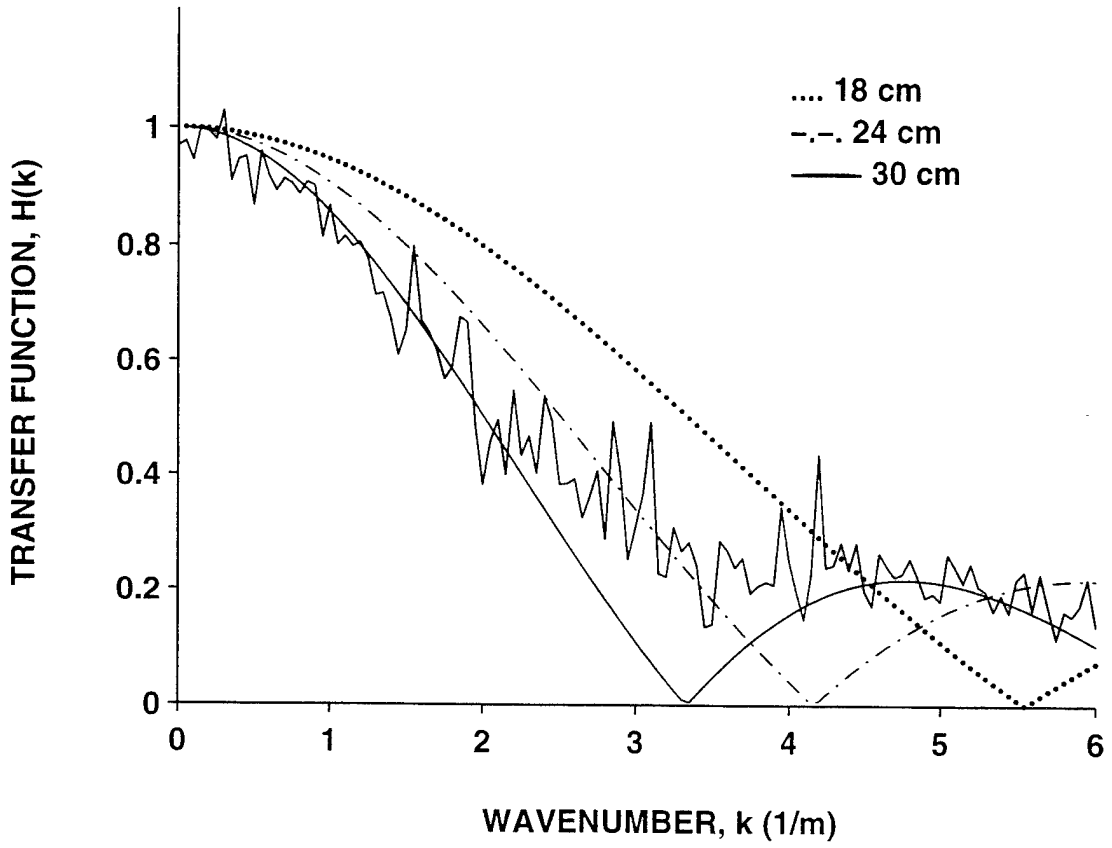

Figure 7. (b) Empirical transfer function of a nine point running median filter calculated using altimeter data compared with the spectral transfers function of a running mean filter with varying averaging lengths.

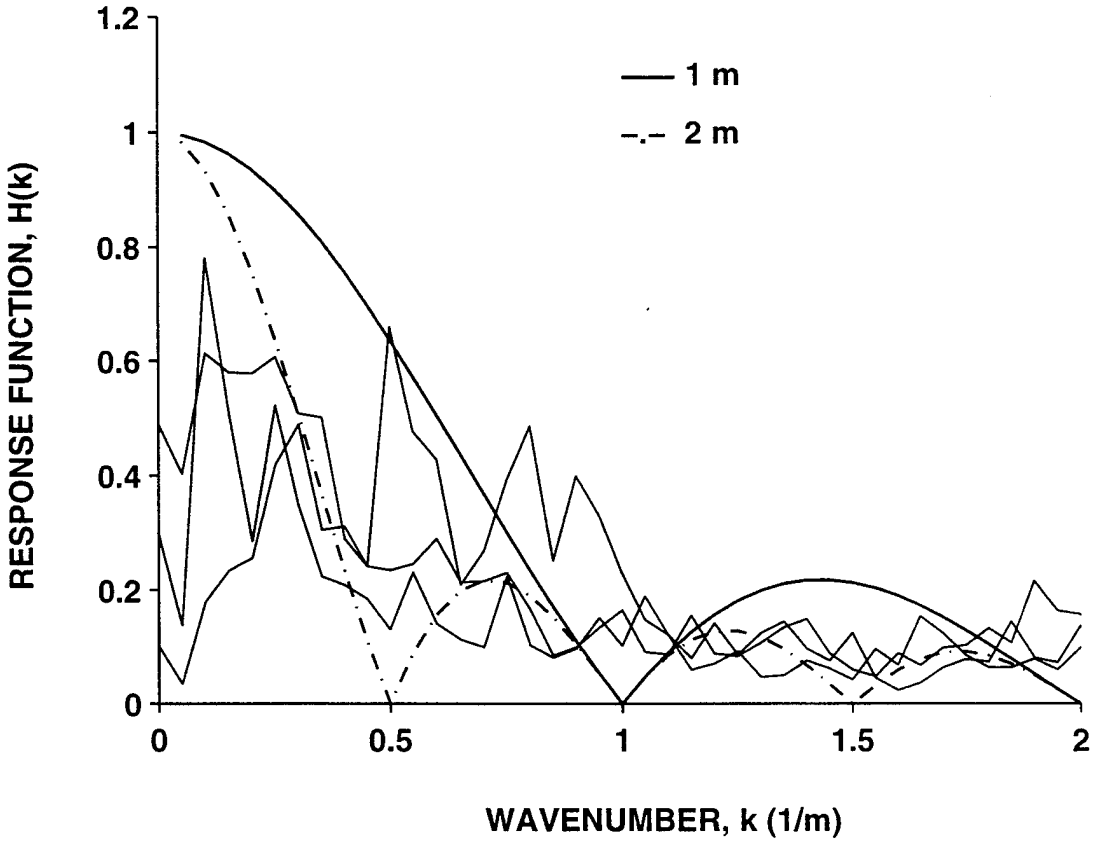

Figure 8. Empirical response function of the CRAB calculated as the ratio of CRAB survey to combined CRAB survey and altimeter data compared with the spectral transfer functions of a running mean filter.

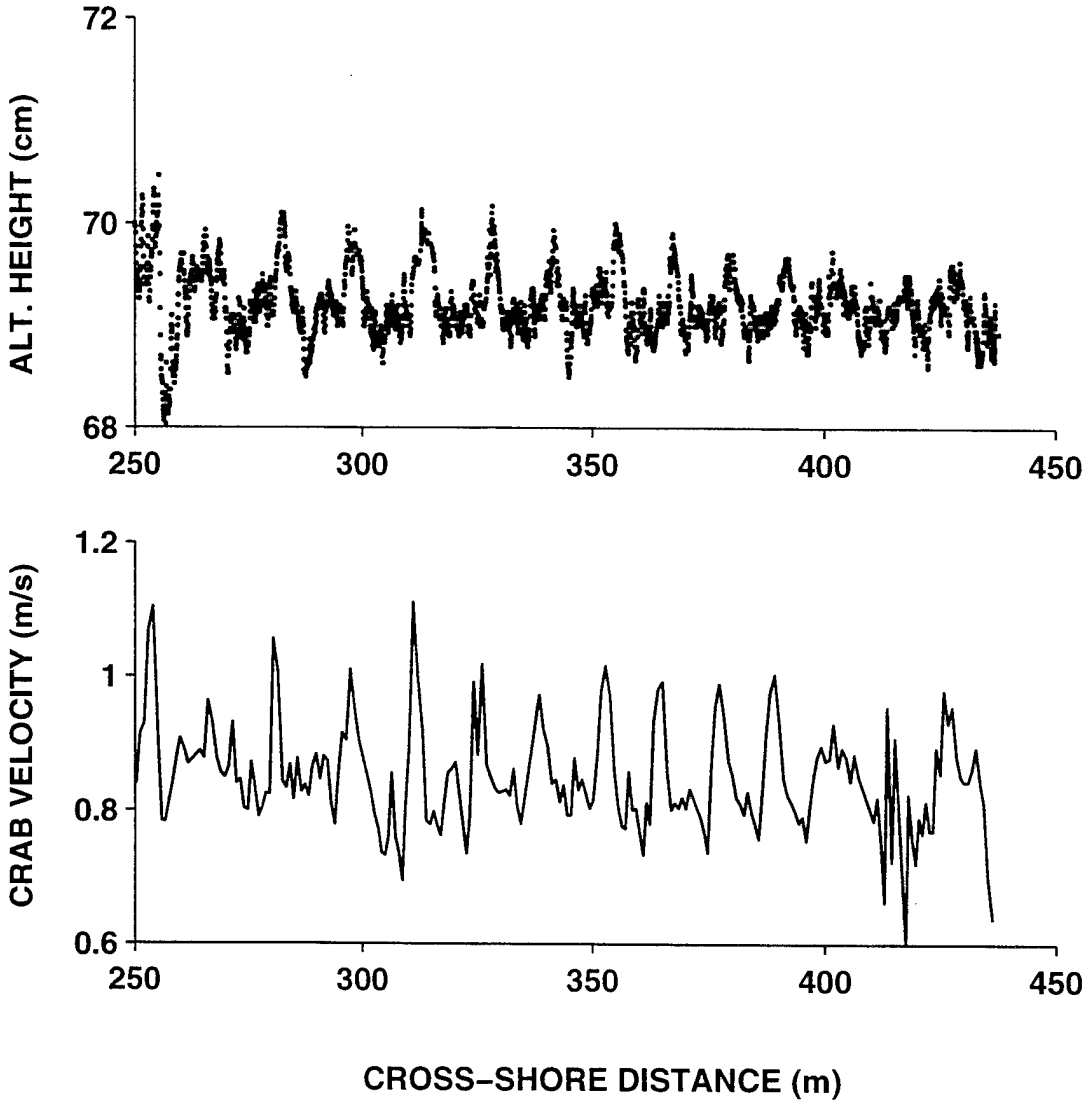

Figure 9. Noise introduced into altimeter data for Oct. 20, line 785 due to the interaction of the CRAB with narrow banded swell (upper panel). CRAB velocity versus cross-shore distance for Oct. 20, line 785 (lower panel).

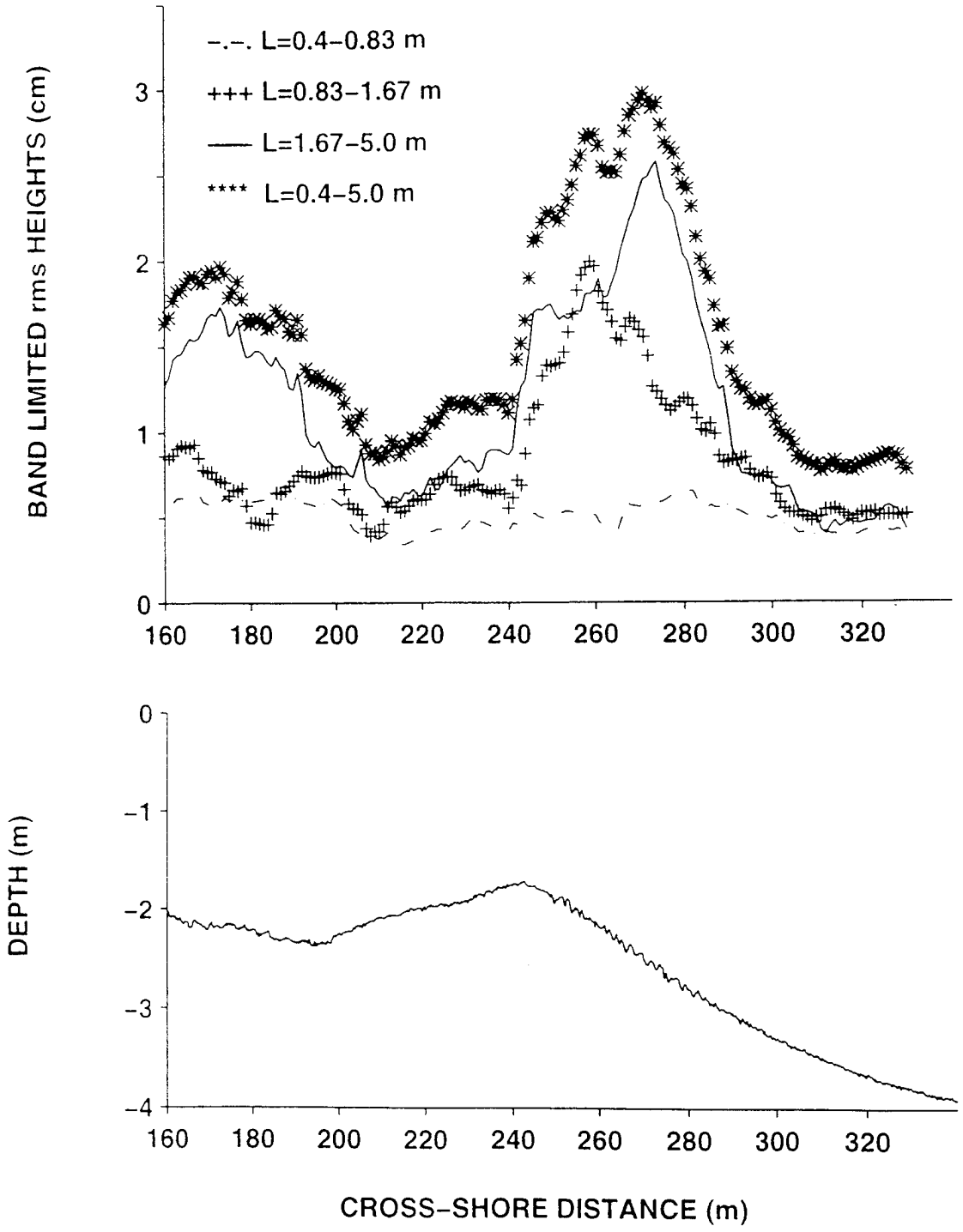

Figure 10. Band limited rms heights calculated across line 940 for Oct. 8 (upper panel). Combined CRAB and altimeter profile of line 940 for Oct. 8 (lower panel).

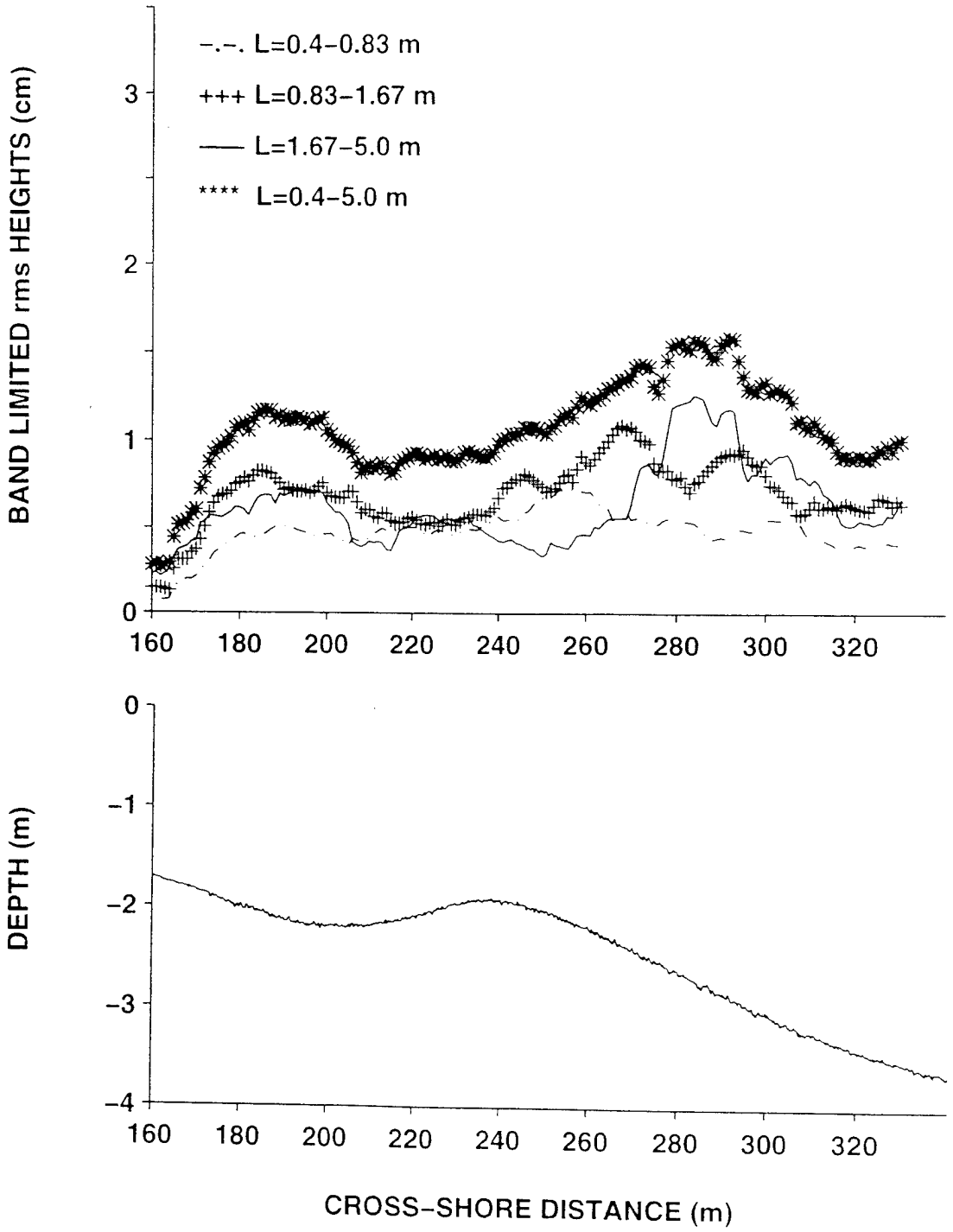

Figure 11. Band limited rms heights calculated across line 710 for Oct. 8 (upper panel). Combined CRAB and altimeter profile of line 710 for Oct. 8 (lower panel).

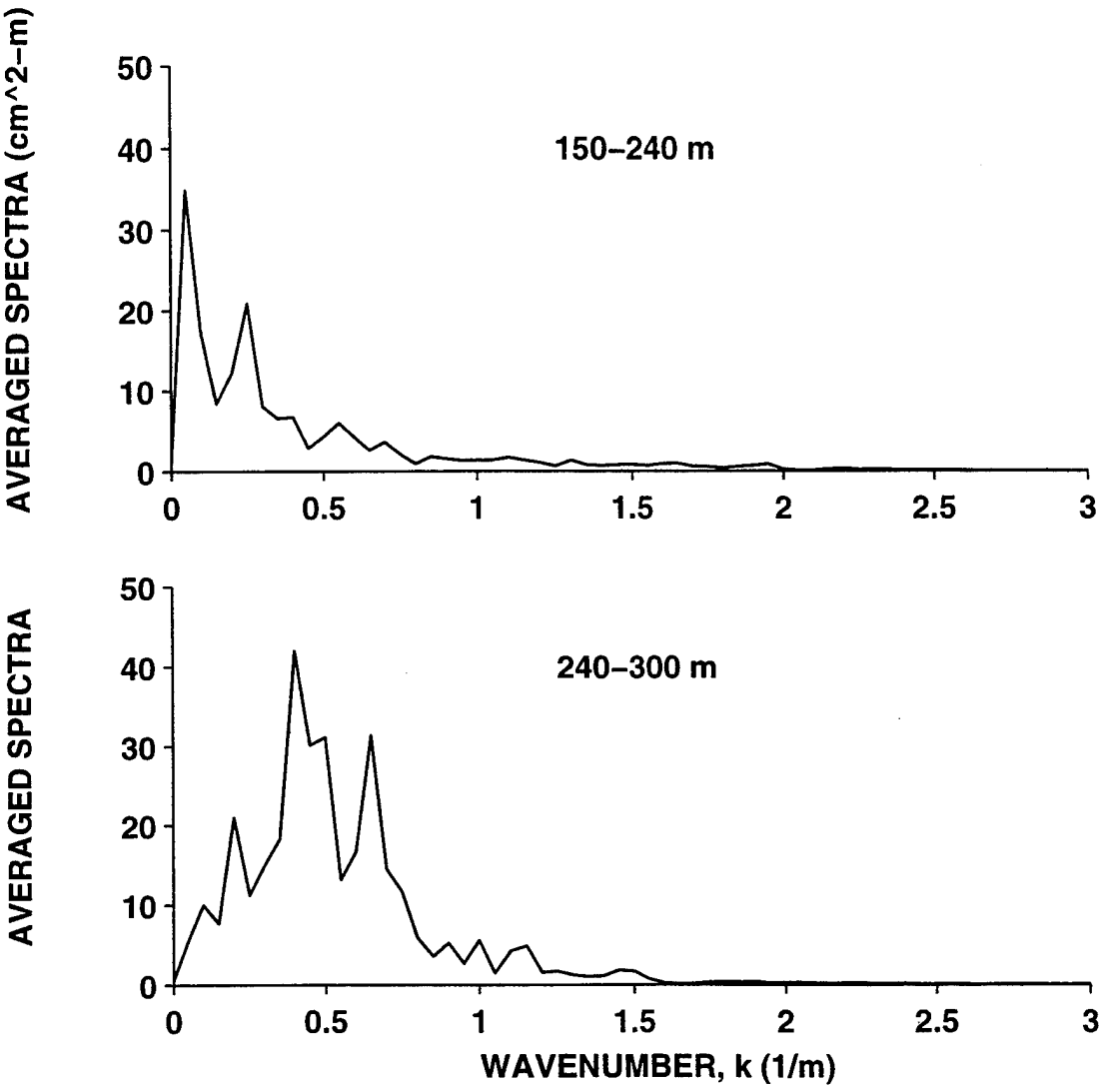

Figure 12. Averaged wavenumber spectra in the trough region and seaward slope of the bar region for line 940 for Oct. 8.

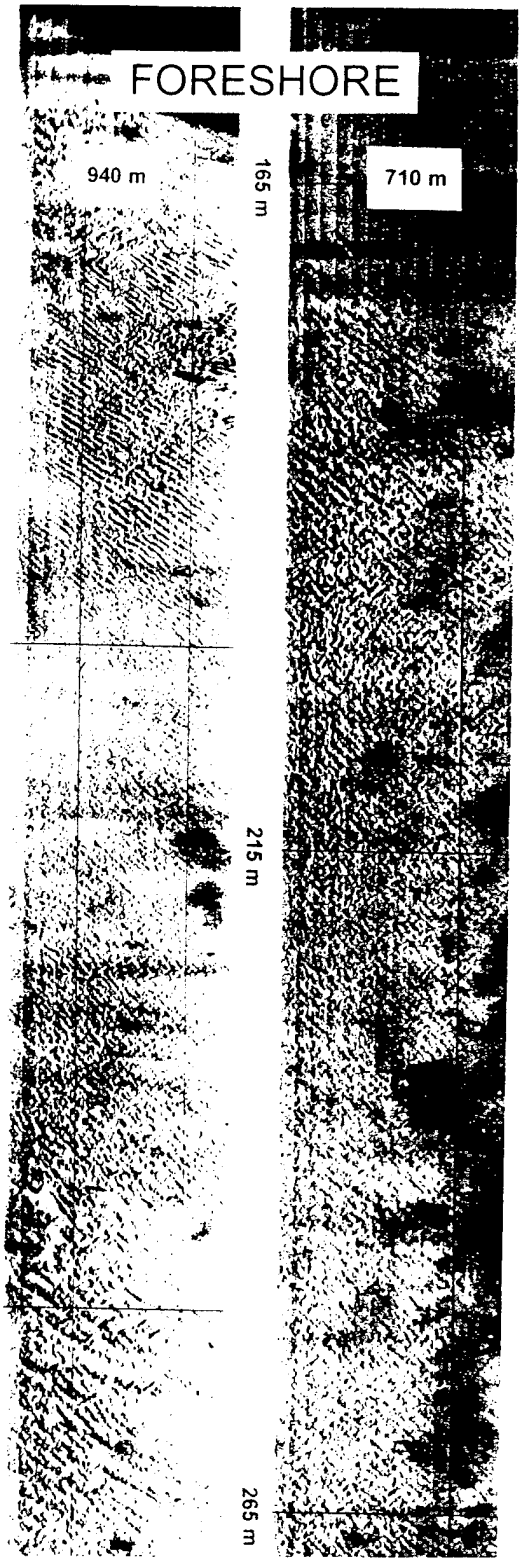

Figure 13. Side-scan sonar plot for lines 940 and 710 for Oct. 8.

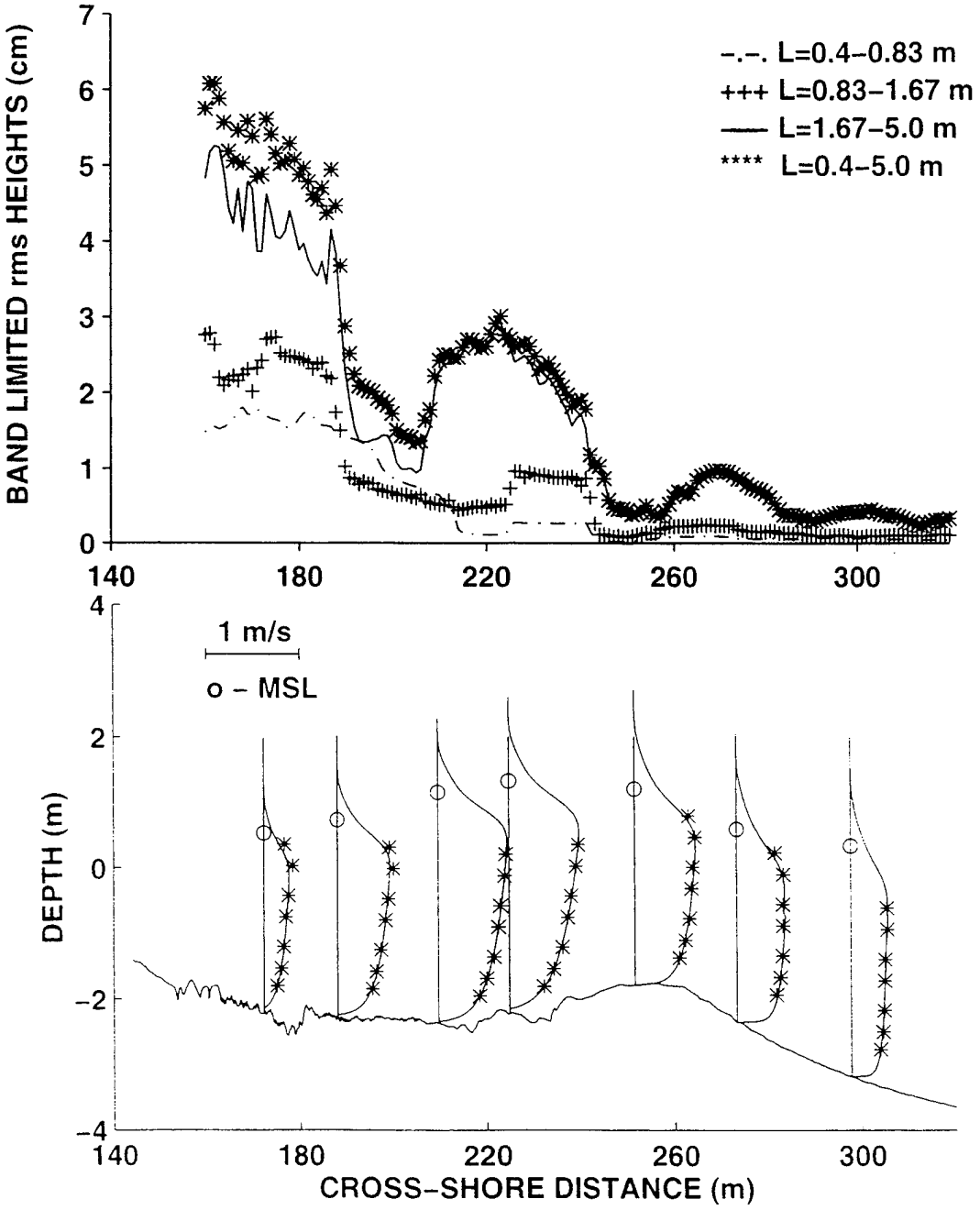

Figure 14. Band limited rms heights calculated across line 940 for Oct. 12 (upper panel). Combined CRAB and altimeter profile of line 940 superimposed with longshore current profiles measured from an instrumented sled for Oct. 12 (lower panel). MSL refers to the mean-sea-level at the time of measurements.

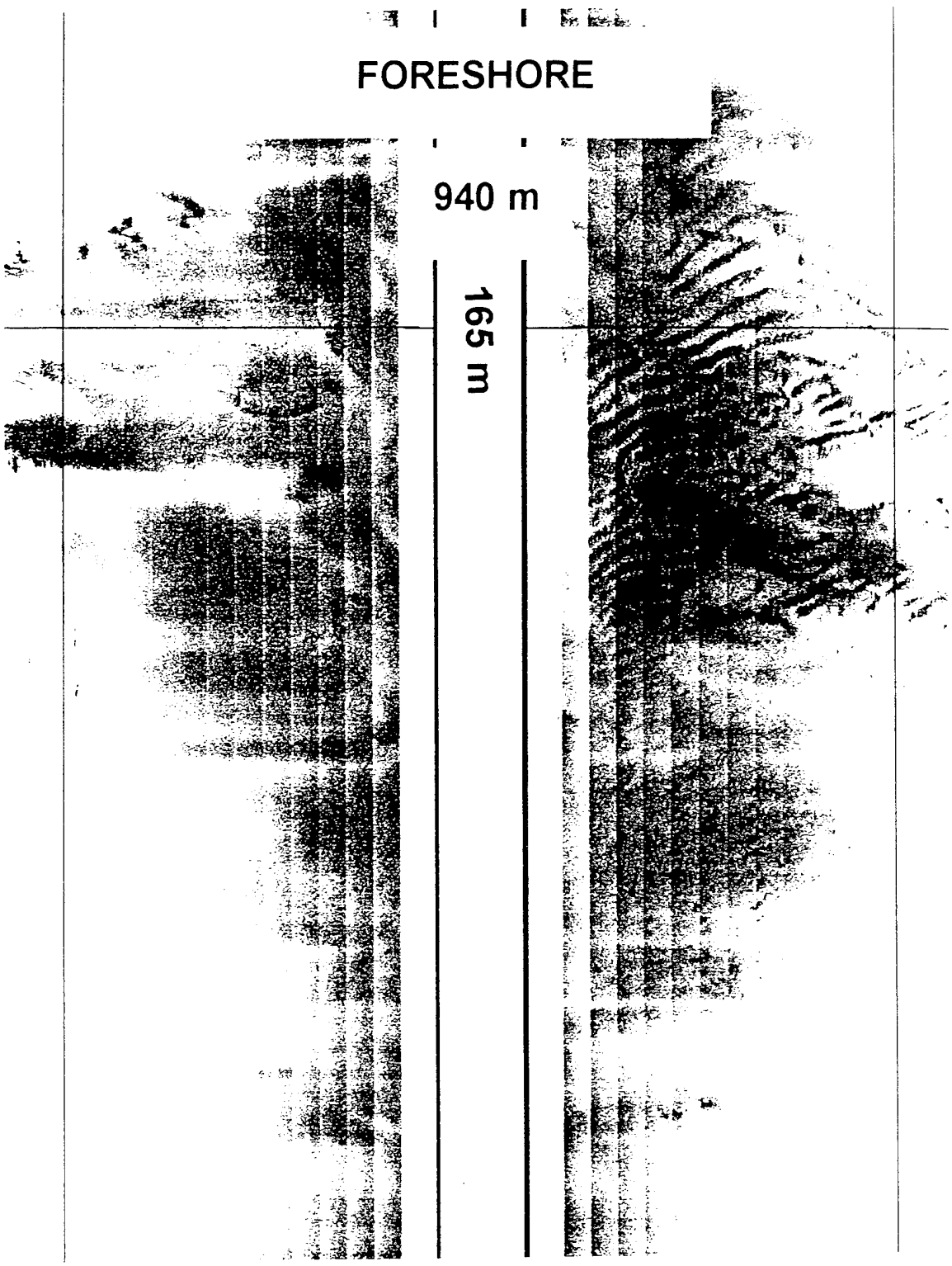

Figure 15. Side-scan sonar plot for line 940 for Oct. 12.

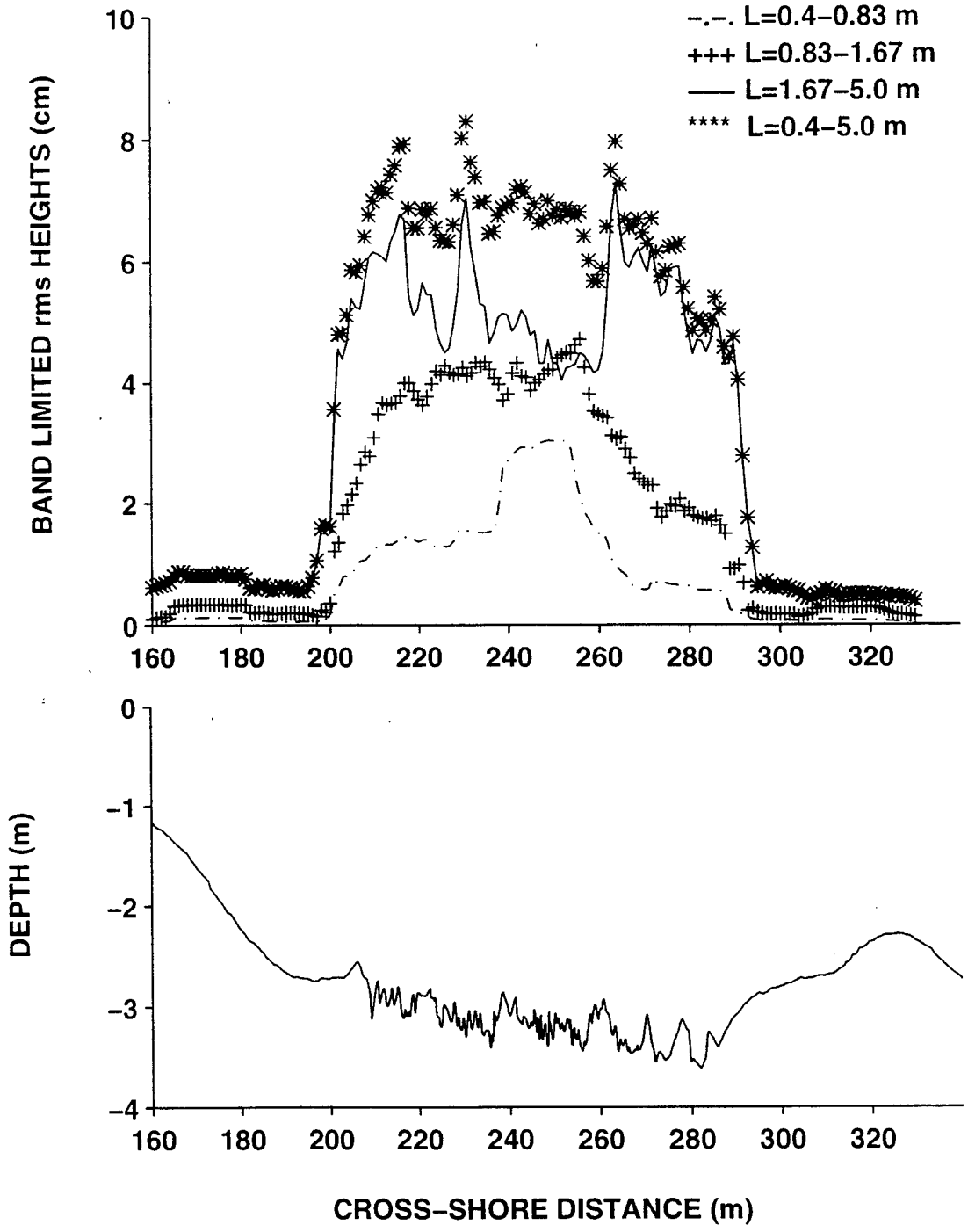

Figure 16. Band limited rms heights calculated across line 1030 for Oct. 20 (upper panel). Combined CRAB and altimeter profile of line 1030 for Oct. 20 (lower panel).

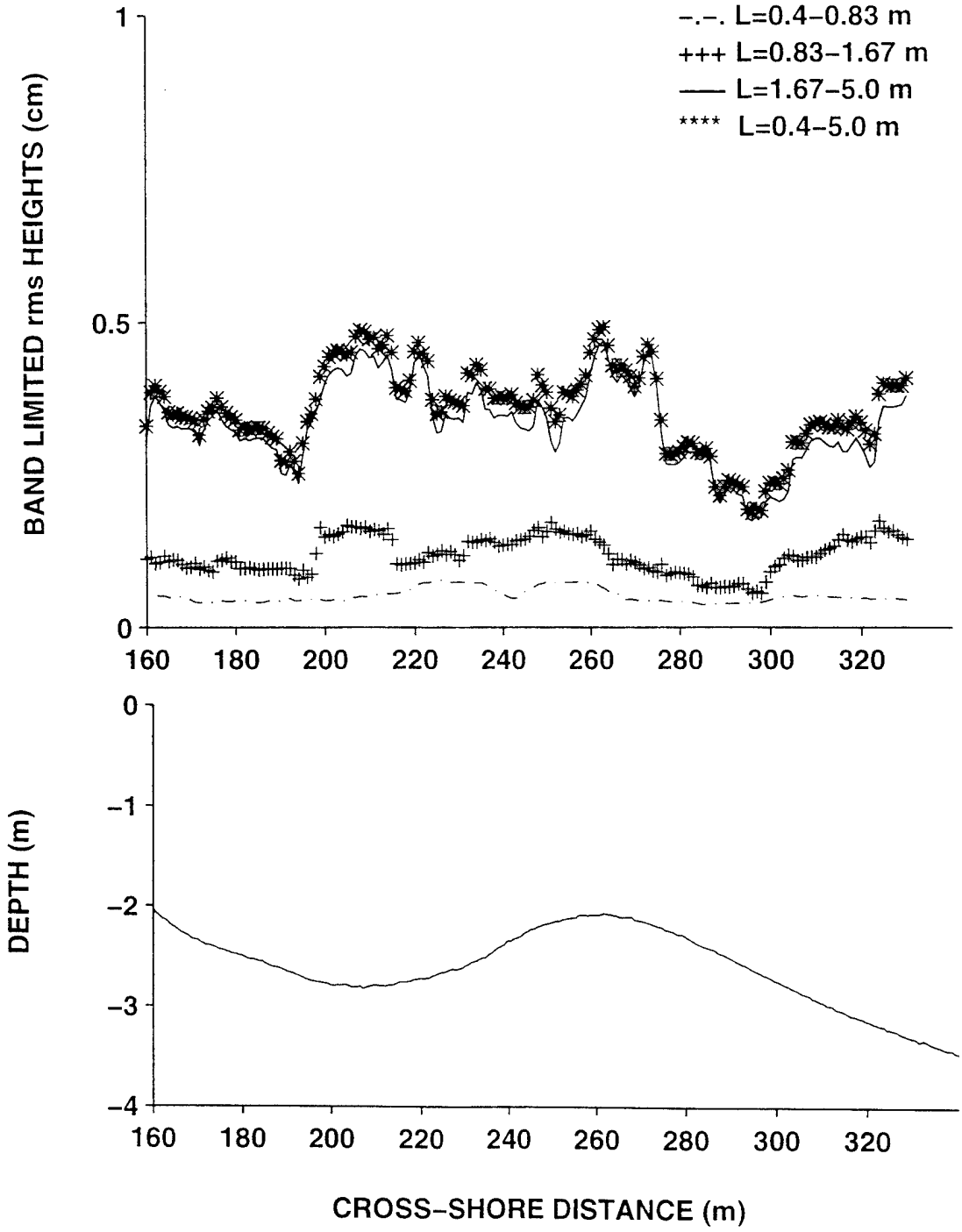

Figure 17. Band limited rms heights calculated across line 785 for Oct. 20 (upper panel). Combined CRAB and altimeter profile of line 785 for Oct. 20 (lower panel).

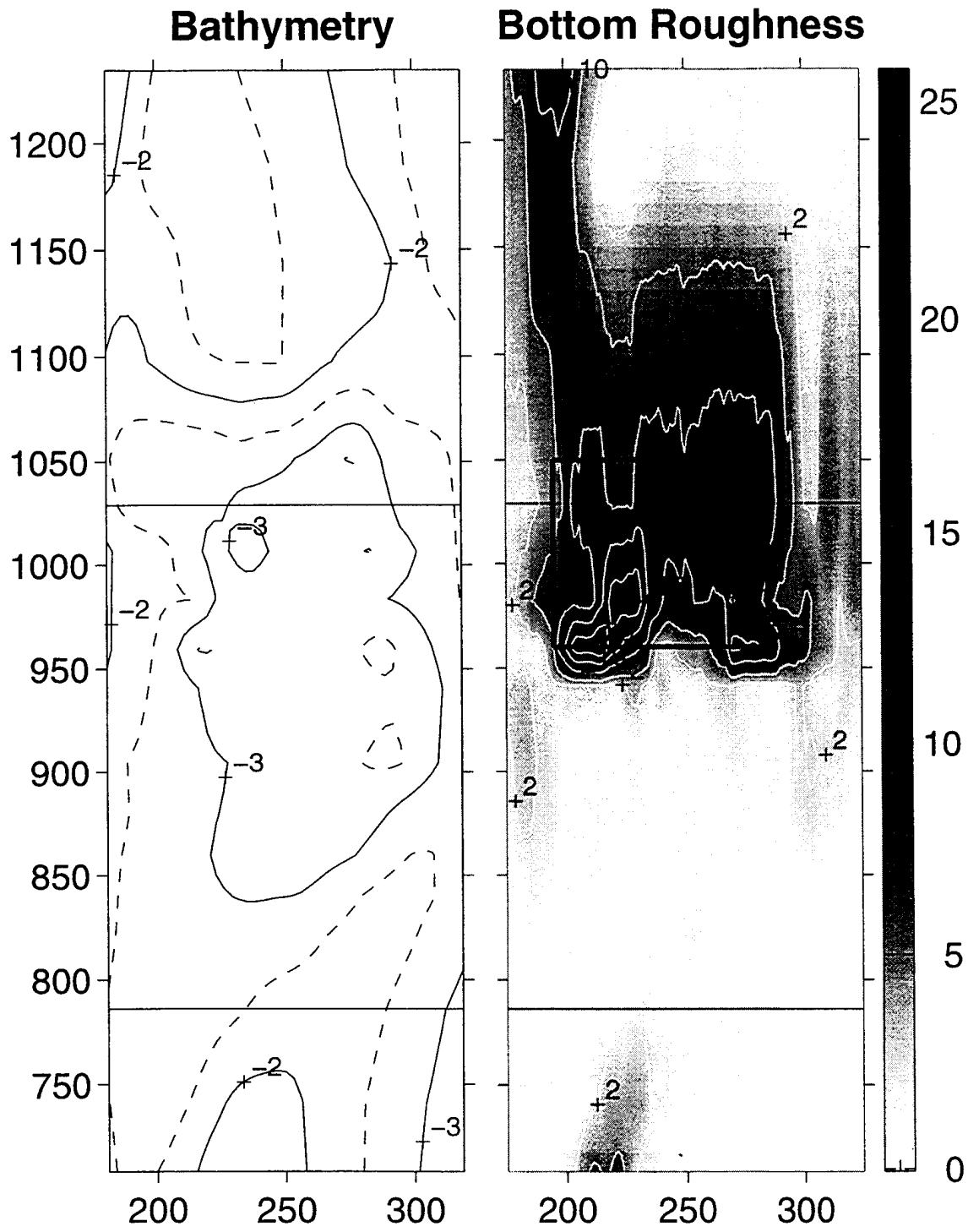

Figure 18. Bathymetry contour plot of DUCK94 survey area for Oct. 20 (left plot). Contour levels are in meters. Rip current is qualitatively indicated based on dye observations. Bottom rms roughness contour plot of survey area for Oct. 20 (right plot). Contour levels are in centimeters. Square indicates area encompassed by side-scan sonar plot in Fig. 19.

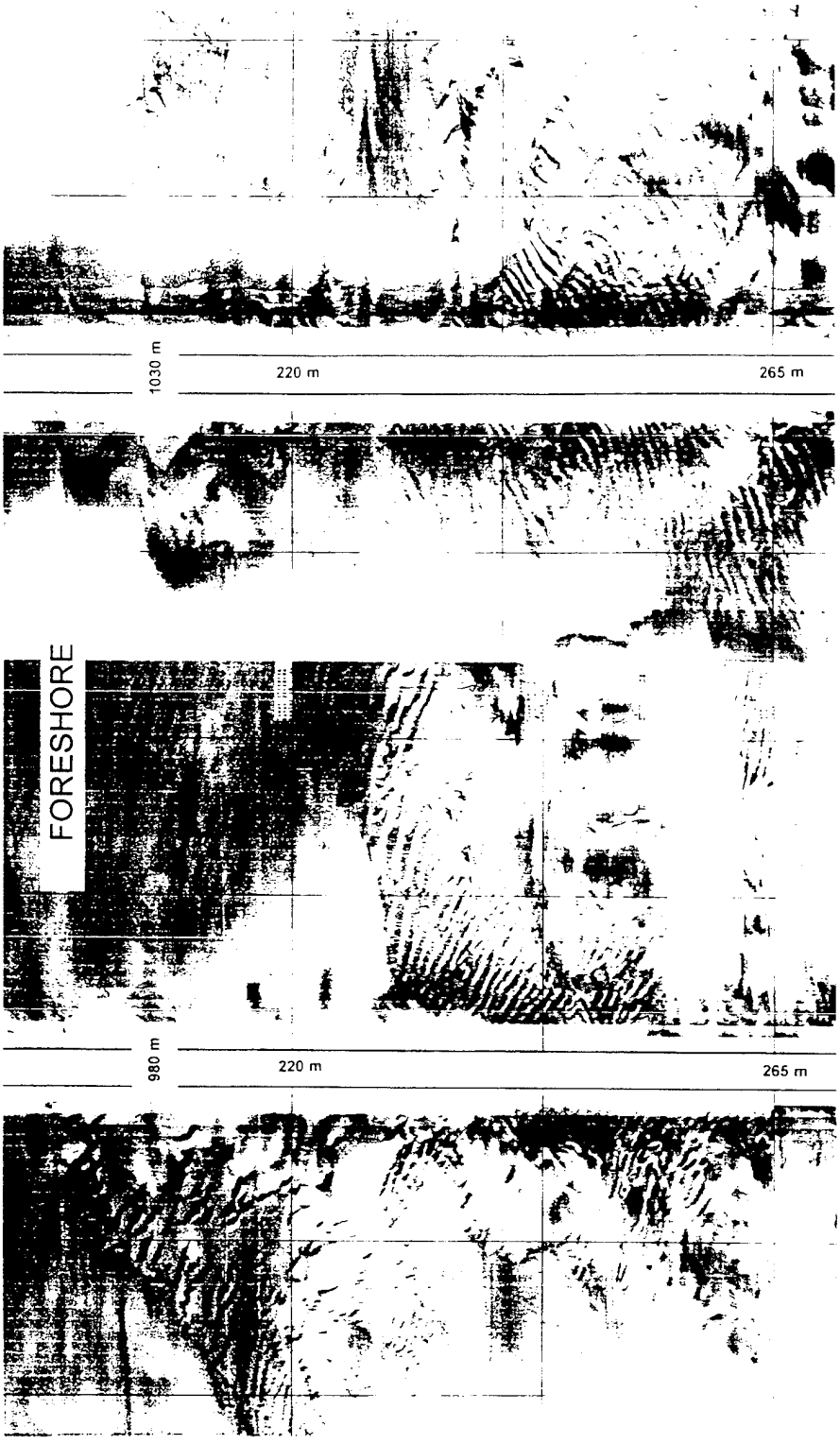

Figure 19. Side-scan sonar plot encompassing the rip-current area for Oct. 20.

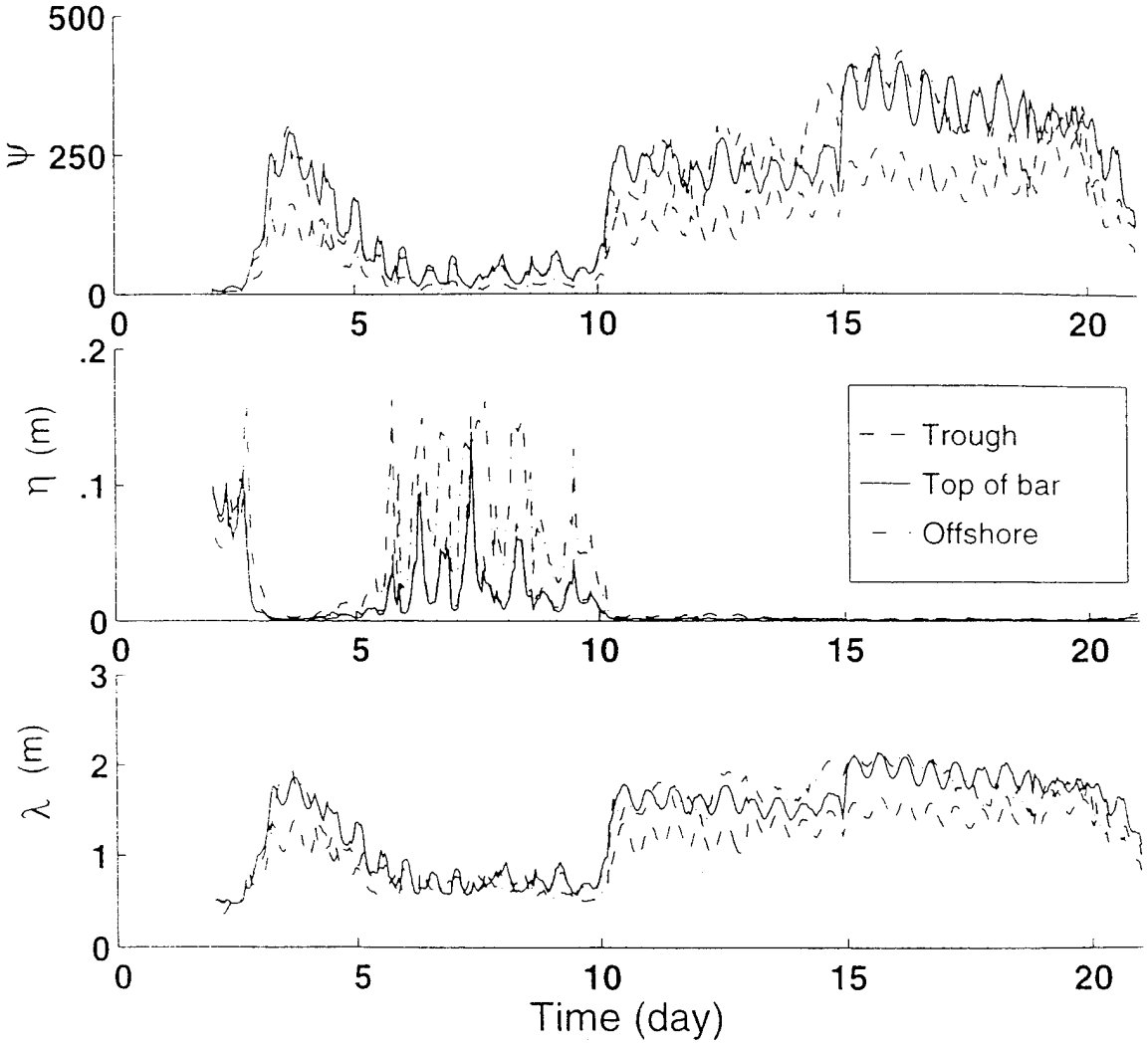

Figure 20. Time series of ψ (Eq. 4), predicted ripple height, η (Eq. 2), and predicted ripple wavelength, λ (Eq. 3) for Oct. 2-20.

REFERENCES

Amos, C.L., Bowen, A.J., Huntley, D.A., and Lewis, C.F.M., 1988. Ripple generation under the combined influences of waves and currents on the Canadian continental shelf. *Continental Shelf Research*, 60(2), 211-219.

Birkemeier, W.A., and Mason, C., 1978. The CRAB: a unique nearshore surveying vehicle. *J. of Survey Engineering, ASCE*, 110(1), 1-7.

Clifton, H.E., Hunter, R.E. and Phillips, R.L., 1971. Depositional structures and processes in the non-barred high-energy nearshore. *J. of Sedimentary Petrology*, 41 (3), 651-670.

Clifton, H.E., 1976. Wave-formed sedimentary structures-A conceptual model. In Davis and Ethington ed: *Beach and Nearshore Sedimentation, SEPM Special Publication*, 24, 126-148.

Davidson-Arnott, R.G.D., and Greenwood, B., 1976. Facies relationships on a barred coast, Kouchibouguard Bay, New Brunswick, Canada. In Davis and Ethington ed: *Beach and Nearshore Sedimentation, SEPM Special Publication*, 24, 149-168.

Davis, R.A., and Fox, W.T., 1972. Coastal processes and nearshore sand bars. *J. Sedimentary Petrology*, 42, 401-412.

Dingler, J.R. and Inman, D.L., 1976. Wave formed ripples in seashore sands. In: *Proceedings 15th Coastal Engineering Conference, ASCE*, pp. 2109-2126.

Gallagher, E.L., Boyd, W., Elgar, S., Guza, R.T., and Woodward, B., 1995. A performance of a sonar altimeter in the nearshore. Submitted to: *Marine Geology*, April 1995.

Hunter, R.E., Clifton, H.E., and Phillips, R.L., 1979. Depositional processes, sedimentary structures, and predicted vertical sequences in barred nearshore systems, Southern Oregon Coast. *J. of Sedimentary Petrology*, 49(3), 711-726.

Lippman, T.C., Holman, R.A., and Hathaway, K.K., 1993. Episodic, nonstationary behavior of a double bar system at Duck, North Carolina, U.S.A., 1986-1991. *J. of Coastal Research*, 15(SI), 49-75.

Miller, M.C., and Komar, P.D., 1980. Afield investigation between oscillation ripple spacing and the near-bottom water orbital motions. *J. Sedimentary Petrology*, 50, 180-191.

Nielsen, P., 1981. Dynamics and geometry of wave-generated ripples. *J. of Geophysical Research*, 86, 6467-6472.

Sherman, D.J., Short, A.D., and Takeda, I., 1993. Sediment mixing-depth and bedform migration in rip channels. *J. of Coastal Research*, 15(SI), 39-48.

Southard, J.B., Lambrie, J.M., Federico, D.C., Pile, H.T., and Weidman, C.R., 1989. Experiments on bed configurations in fine sands under bidirectional purely oscillatory flow, and the origin of hummocky cross-stratification. *J. Sedimentary Petrology*, 60(1), 1-17.

Thornton, E.B, and Guza, R.T., 1983. Transformation of wave height distribution. *J. Geophysical Research*, 88(C10), 5925-5938.

Van Rijn, L.C., and Havinga, F.J., 1995. Transport of fine sands by currents and waves. *J. of Waterway, Port, Coastal, and Ocean Engineering*, 121(2), 123-132.

INITIAL DISTRIBUTION LIST

		No. Copies
1.	Defense Technical Information Center 8725 John J. Kingman Rd., STE 0944 Ft. Belvoir, VA 22060-6218	2
2.	Library, Code 13 Naval Postgraduate School Monterey, California 93943-5101	2
3.	Oceanography Department Code OC/Co Naval Postgraduate School 833 Dyer Rd. Rm. 331	1
4.	Prof E.B. Thornton Oceanography Department Code OC/Tm Naval Postgraduate School 833 Dyer Rd. Rm. 331	2
5.	LT J.L. Swayne Naval Atlantic Meteorology and Oceanography Center 9141 Third Ave. Norfolk, VA 23511-2394	2
6.	Prof. T. Lippmann Scripps Institute of Oceanography La Jolla, CA 92037	1
7.	Commander Naval Oceanography Command Stennis Space Center, MS 39529-5000	1